HHS Public Access

Author manuscript

Neuron. Author manuscript; available in PMC 2018 July 19.

Published in final edited form as:

Neuron. 2017 July 19; 95(2): 326–340.e5. doi:10.1016/j.neuron.2017.06.018.

Retrograde synaptic inhibition is mediated by α-Neurexin binding to the α2δ subunits of N-type calcium channels

Xia-Jing Tong[1,2], **Eduardo Javier López-Soto**[4], **Lei Li**[5], **Haowen Liu**[5], **Daniel Nedelcu**[1,2], **Diane Lipscombe**[4], **Zhitao Hu**[5], and **Joshua M. Kaplan**[1,2,3,*]

[1]Department of Molecular Biology, Massachusetts General Hospital, Boston, MA 02114, USA

[2]Department of Neurobiology, Harvard Medical School, Boston, MA 02115, USA

[3]Program in Neuroscience, Harvard Medical School

[4]Department of Neuroscience and Brown Institute for Brain Science, Brown University, Providence, RI 02912

[5]Clem Jones Centre for Ageing Dementia Research, Queensland Brain Institute, The University of Queensland, Brisbane, Australia

Summary

The synaptic adhesion molecules Neurexin and Neuroligin alter the development and function of synapses and are linked to autism in humans. In *C. elegans*, post-synaptic Neurexin (NRX-1) and pre-synaptic Neuroligin (NLG-1) mediate a retrograde synaptic signal that inhibits acetylcholine (ACh) release at neuromuscular junctions. Here we show that the retrograde signal decreases ACh release by inhibiting the function of pre-synaptic UNC-2/CaV2 calcium channels. Post-synaptic NRX-1 binds to an auxiliary subunit of pre-synaptic UNC-2/CaV2 channels (UNC-36/α2δ) decreasing UNC-36 abundance at pre-synaptic elements. Retrograde inhibition is mediated by a soluble form of NRX-1's ectodomain, which is released from the post-synaptic membrane by the SUP-17/ADAM10 protease. Mammalian Neurexin-1α binds α2δ–3 and decreases CaV2.2 current in transfected cells whereas Neurexin-1α has no effect on CaV2.2 reconstituted with α2δ1 and α2δ2. Collectively, these results suggest that α-Neurexin binding to α2δ is a conserved mechanism for regulating synaptic transmission.

*Lead contact. Correspondence to: kaplan@molbio.mgh.harvard.edu.

Author Contributions

X-J.T, E.L-S., L.L., H.L., and D.N. designed, performed, and analyzed the experiments. X-J.T performed all *C. elegans* imaging studies and characterized α-NX binding to α2δ proteins; E.L-S. analyzed mammalian CaV2.2 currents in tsA201 cells; L.L. and H.L. performed *C. elegans* electrophysiological recordings; D.N. purified recombinant btNX-1α; D.L., Z.H., and J.K. supervised the design and data interpretation; J.K. wrote the manuscript. All authors discussed the results and commented on the manuscript.

Introduction

Synaptic transmission is mediated by exocytosis of synaptic vesicles (SVs), which are filled with neurotransmitter. SV fusion is triggered by a local calcium transient, produced by activation of pre-synaptic voltage-gated calcium channels (CaVs). Secreted neurotransmitter activates receptors embedded in the post-synaptic membrane, thereby depolarizing or hyperpolarizing post-synaptic cells.

Synaptic signals occur with extremely high spatial and temporal precision. Fusion of SVs in presynaptic terminals is restricted to a spatial domain extending ~300 nm from activated CaVs (Watanabe et al., 2013). Similarly, post-synaptic receptor activation is limited to a domain extending ~100 nm from the site of SV fusion (Raghavachari and Lisman, 2004). Given these tiny spatial domains, post-synaptic currents are activated ~150 μs after the presynaptic action potential (Sabatini and Regehr, 1996). The extreme spatial and temporal precision of synaptic transmission are likely a consequence of tight physical coupling of pre- and post-synaptic specializations.

Physical coupling of the pre- and post-synaptic cells is mediated by trans-synaptic adhesion molecules. Over the past several years, several families of synaptic adhesion molecules have been identified. Among these, Neurexin (NX) and Neuroligin (NL) proteins play a prominent role. Mammals have three NX genes, each encoding long (α) and short (β) isoforms, and four NL genes. Mammalian NX proteins are typically presynaptic while NL proteins are post-synaptic. When expressed in non-neuronal cells, NX induces formation of post-synaptic elements in contacting neurons whereas NL induces pre-synaptic elements (Graf et al., 2004; Nam and Chen, 2005; Scheiffele et al., 2000). NX and NL's synaptogenic activities are thought to be mediated by induced clustering of pre- and post-synaptic proteins caused by trans-synaptic contact (Dean et al., 2003).

Because they form a physical link across the synapse, NX and NL have the capacity to mediate bi-directional signaling between pre- and post-synaptic cells. Consistent with this idea, pre-synaptic NX has been shown to promote clustering of post-synaptic $GABA_A$, AMPA, and NMDA receptors (Aoto et al., 2013; Heine et al., 2008; Kang et al., 2008; Nam and Chen, 2005; Tong et al., 2015). By controlling post-synaptic receptor abundance, pre-synaptic NX plays an important role in regulating the strength of synaptic signals (i.e. by directly altering the size of quantal responses).

Other studies suggest that post-synaptic NL alters pre-synaptic properties. Over-expression of NL or PSD95 (which binds NL) increases formation of trans-synaptic NX-NL complexes and increases release probability in rat hippocampal neurons (Futai et al., 2007; Wittenmayer et al., 2009). Post-synaptic NL3 decreases excitatory input to parvalbumin expressing interneurons in the CA1 region of the hippocampus (Polepalli et al., 2017). These studies support the idea that NX-NL signaling regulates presynaptic function; however, little is known about the biochemical basis for these presynaptic effects.

To address this question, we have studied a *C. elegans* retrograde signal whereby muscles inhibit acetylcholine (ACh) release from motor neurons at neuromuscular junctions (NMJs) (Simon et al., 2008). This retrograde signal is induced by inactivation of a muscle

microRNA (miR-1) and is abolished by mutations inactivating the transcription factor MEF-2 (a miR-1 target), or those inactivating NRX-1/α-NX and NLG-1/NL (Hu et al., 2012; Simon et al., 2008). At this synapse, NL is pre-synaptic and NX is post-synaptic, opposite to the polarity observed at mammalian synapses. Other examples of reversed polarity include presynaptic NLG-1 in worms (Feinberg et al., 2008; Hunter et al., 2010) and post-synaptic mouse and fly NX (Chen et al., 2010; Kattenstroth et al., 2004; Taniguchi et al., 2007). This flipped polarity is not observed at all *C. elegans* synapses. For example, at GABAergic NMJs, NRX-1 and NLG-1 are pre-and post-synaptic, respectively (Maro et al., 2015; Tong et al., 2015; Tu et al., 2015). Here we show that post-synaptic NRX-1 inhibits ACh release by directly binding to and inhibiting the function of α2δ subunits associated with pre-synaptic N-type (CaV2) calcium channels.

Results

UNC-2/CaV2 and EGL-19/CaV1 both contribute to synaptic transmission at cholinergic NMJs

Because the retrograde signal inhibits ACh release, we hypothesized that trans-synaptic NX-NL complexes regulate pre-synaptic voltage-activated calcium (CaV) channels. To test this idea, we first asked which CaVs are responsible for ACh release at NMJs. The *C. elegans* genome encodes one N-type (UNC-2/CaV2) and one L-type (EGL-19/CaV1) calcium channel. How these CaVs contribute to synaptic transmission has not been fully characterized (Fig. 1A). To block release coupled to UNC-2/CaV2, we analyzed excitatory post-synaptic currents (EPSCs) in *unc-2* null mutants. Because *egl-19* null mutants are inviable, we utilized an antagonist (Nemadipine) to block EGL-19/CaV1 mediated release (Kwok et al., 2006). Nemadipine treatment (10 μM) completely blocked voltage-activated EGL-19/CaV1 calcium current in body muscles (Fig. S1A–B), confirming that Nemadipine is an effective EGL-19 antagonist (Laine et al., 2011).

Using these tools, we asked if UNC-2 and EGL-19 are required for ACh release at NMJs. Transmission at this synapse is mediated by graded ACh release, whereby release varies with the strength of depolarization (Liu et al., 2009). When activity is low, transmission consists of spontaneous miniature excitatory post-synaptic currents (mEPSCs) that result from single SV fusions (Liu et al., 2005), hereafter designated tonic release. Direct depolarization of motor neurons evokes the synchronous release of several hundred SVs.

Which CaV is required for evoked ACh release? Evoked EPSCs were nearly completely eliminated in *unc-2* null mutants, whereas the amplitude of evoked responses was unaffected by Nemadipine treatment (Fig. 1B–C). Thus, the vast majority of SV fusions during evoked responses are coupled to UNC-2/CaV2.

Next, we asked which CaV mediates tonic ACh release. The mEPSC rate was significantly reduced in *unc-2* mutants (57% WT) and by Nemadipine treatment (60% untreated controls) (Fig. 1B,D). mEPSCs were nearly completely eliminated in Nemadipine treated *unc-2* mutants (Fig. 1B,D). mEPSC amplitudes were unaltered in *unc-2* mutants and in Nemadapine treated animals (Fig. 1E), suggesting that muscle sensitivity to ACh had not been altered. To confirm EGL-19's role in promoting tonic release, we constructed

transgenic animals in which an *egl-19* null mutation is complemented by a transgene that restores EGL-19 expression only in body muscles [designated EGL-19(N^-M^+)]. Compared to wild type controls, the mEPSC rate was significantly reduced in EGL-19(N^-M^+) animals and was not further reduced by Nemadapine treatment (Fig. S1C–D). These results confirm that EGL-19/CaV1 functions in neurons to promote ACh release and that Nemadapine's effects on mEPSC rate are mediated by inhibiting EGL-19 function in neurons. Thus, tonic ACh release comprises a mixture of SV fusions coupled to both UNC-2/CaV2 and EGL-19/CaV1.

UNC-36/α2δ is required for UNC-2/CaV2 but not EGL-19/CaV1 mediated ACh release

CaVs are heteromeric complexes containing pore forming (α1) and auxiliary (β and α2δ) subunits. Mammals have four predicted α2δ encoding genes (CACNA2D1–4). α2δ subunits play redundant roles promoting CaV1 and 2 trafficking to (and retention in) the plasma membrane (Bernstein and Jones, 2007; Canti et al., 2005; Dolphin et al., 1999). α2δ subunits also have modest effects on gating, accelerating inactivation and deactivation of CaV1 and 2 (Felix et al., 1997; Klugbauer et al., 1999). In rat hippocampal neurons, α2δ-1 localizes CaV2.1 or CaV2.2 in the active zone, thereby promoting the coupling of CaV2 to SV exocytosis and enhancing synaptic transmission (Hoppa et al., 2012).

The *C. elegans* genome encodes two α2δ subunits, UNC-36 and TAG-180. A prior study suggested that UNC-36/α2δ is an essential auxiliary subunit for UNC-2/CaV2 (Saheki and Bargmann, 2009). Mutants lacking UNC-36/α2δ have a behavioral phenotype very similar to *unc-2* mutants and *unc-36* mutants have a dramatic decrease in the pre-synaptic localization of GFP-tagged UNC-2 channels (Saheki and Bargmann, 2009). Conflicting results have been reported for UNC-36 effects on EGL-19/CaV1 channels (Laine et al., 2011; Gao and Zhen, 2011).

To determine if UNC-36 is required for UNC-2 and EGL-19 function in neurons, we recorded tonic and evoked EPSCs from *unc-36* mutants. We found that *unc-36* and *unc-2* mutants exhibit very similar electrophysiological phenotypes. Evoked EPSCs (which consist of SV fusions coupled to UNC-2/CaV2) were dramatically reduced in *unc-36* mutants (Fig. 1B–C). Tonic release (which is mediated by both UNC-2 and EGL-19) was reduced but not eliminated in *unc-36* mutants (Fig. 1B,D). The residual mEPSCs in *unc-36* mutants were eliminated by Nemadipine treatment, indicating that *unc-36* mutations decreased tonic release coupled to UNC-2/CaV2 channels (Fig. 1B,D). The mEPSC rate observed in *unc-36; unc-2* double mutants was indistinguishable from that found in either single mutant (Fig. 1D), suggesting that UNC-36/α2δ effects on mEPSC rate are mediated by altered UNC-2/CaV2 function. Collectively, these results suggest that UNC-36/α2δ subunits are required for the function of pre-synaptic UNC-2/CaV2 but not for EGL-19/CaV1.

UNC-36/α2δ synaptic localization is mediated by binding to endogenous UNC-2/CaV2

If UNC-36/α2δ is an auxiliary subunit for UNC-2/CaV2, UNC-36 should be localized to pre-synaptic terminals. To visualize UNC-36 localization, we constructed a chimeric protein (mngUNC-36) in which a fluorescent protein (mNeonGreen) was inserted after the amino-terminal signal peptide sequence. A transgene expressing mngUNC-36 in all neurons (using

the *snb-1* promoter) rescued *unc-36* mutant defects in synaptic transmission (Fig. 2A), suggesting that the fluorescent tag did not interfere with UNC-36 function. To determine its subcellular localization, we expressed mngUNC-36 in the DA and DB cholinergic motor neurons (using the *unc-129* promoter). DA/DB neurons receive synaptic input in the ventral nerve cord (VNC), and form NMJs with body muscles in the dorsal nerve cord (DNC) (White et al., 1986). Thus, expression in DA/DB neurons provides a simple means for distinguishing axonal (DNC) and dendritic (VNC) protein localization. The mngUNC-36 protein formed fluorescent puncta in the DA/DB dorsal cord axons, whereas diffuse fluorescence was observed in DA/DB ventral cord dendrites. The axonal mngUNC-36 puncta were strongly co-localized with a synaptic vesicle protein (UNC-57/endophilin), confirming that mngUNC-36 is localized to pre-synaptic elements (Fig. 2B, E). The apparent pre-synaptic localization of mngUNC-36 could result from increased axonal volume at pre-synaptic elements. To test this possibility, we compared the subcellular localization of mngUNC-36 with soluble mCherry (also expressed in DA/DB neurons). We found that the axonal puncta fluorescence (measured as ΔF/F) of mngUNC-36 was significantly greater than soluble mCherry (Fig. 2C–D). Similarly, mngUNC-36 co-localization with UNC-57/Endophilin was significantly greater than with mCherry (Fig. 2E). Collectively, these results suggest that mngUNC-36 is enriched at pre-synaptic nerve terminals, and that this synaptic enrichment cannot be accounted for by increased axonal volume at synaptic varicosities.

If mngUNC-36 accumulation at presynaptic terminals is mediated by association with UNC-2/CaV2, mngUNC-36 puncta fluorescence should be diminished in mutants lacking UNC-2/CaV2 channels. Consistent with this idea, mngUNC-36 puncta intensity was significantly reduced in *unc-2* mutants (Fig. 2F–G). Decreased puncta fluorescence in *unc-2* mutants could result from decreased expression of the *unc-129* promoter (which drives mngUNC-36 expression). To address this possibility, we used the *unc-129* promoter to co-express mCherry and mngUNC-36 in DA/DB neurons. We found that mCherry puncta intensity was unaltered in *unc-2* mutants (Fig. S2A–B). When mngUNC-36 puncta fluorescence (ΔF/F) was normalized to the co-expressed mCherry, we observed a significant decrease in mngUNC-36 synaptic enrichment in *unc-2* mutants (Fig. S2C). Thus, the *unc-2* mutation decreased the presynaptic accumulation of mngUNC-36, and this effect cannot be explained by decreased expression of the *unc-129* promoter, nor by a change in the size of synaptic varicosities.

To further test the idea that UNC-36 associates with UNC-2/CaV2, we analyzed *unc-10* RIM mutants. In mouse and fly neurons, the active zone protein RIM is required to localize CaV2 to nerve terminals (Graf et al., 2012; Kaeser et al., 2011). Consequently, if UNC-36 associates with UNC-2/CaV2, *unc-10* mutants should have decreased presynaptic UNC-36 abundance. As expected, mngUNC-36 puncta intensity was significantly reduced in *unc-10* mutants (Fig.2F–G). Decreased synaptic mngUNC-36 levels in *unc-2* and *unc-10* mutants could be a secondary consequence of decreased synaptic transmission in these mutants. To address this possibility, we examined mngUNC-36 fluorescence in *unc-13* mutants, which have a nearly complete block in SV exocytosis (Richmond et al., 1999). We found that mngUNC-36 puncta intensity was not significantly reduced in *unc-13* mutants (Fig. 2F–G), indicating that decreased synaptic transmission cannot account for diminished synaptic

mngUNC-36 levels in *unc-2* and *unc-10* mutants. Thus, mngUNC-36 is localized to pre-synaptic terminals in a manner that requires endogenously expressed UNC-2/CaV2. Collectively, these results support the idea that UNC-36 is an auxiliary subunit that physically associates with pre-synaptic UNC-2/CaV2.

The retrograde signal selectively inhibits release coupled to UNC-2/CaV2

Retrograde inhibition of ACh release could reflect a decrease in SV fusions coupled to UNC-2/CaV2 or EGL-19/CaV1. To distinguish between these possibilities, we analyzed tonic release in *mir-1* mutants lacking either UNC-2 or EGL-19. As previously reported, the mEPSC rate was significantly reduced in *mir-1* mutants (50% WT controls). This effect was abolished in *mir-1; unc-2* double mutants but was unaffected when EGL-19/CaV1 channels were blocked with Nemadipine (Fig. 3A–B). Similarly, the mEPSC rate observed in *mir-1; unc-36* double mutants was indistinguishable from that observed in either single mutant, suggesting that miR-1 and UNC-36/α2δ function together to regulate tonic release (Fig.3C–D). Collectively, these results support the idea that the retrograde signal inhibits tonic release by altering the function of UNC-2/CaV2 while having little effect on release mediated by EGL-19/CaV1.

UNC-36/α2δ binds NRX-1/α-NX

Thus far, our results suggest that the retrograde signal (which is mediated by trans-synaptic NLG-1/NRX-1 complexes) (Hu et al., 2012) inhibits synaptic transmission by selectively inhibiting release coupled to UNC-2/CaV2. A simple model to explain these results would be that NLG-1/NRX-1 complexes directly interact with pre-synaptic UNC-2. Because α2δ subunits have an extensive extra-cellular domain that extends into the synaptic cleft, we hypothesized that post-synaptic NRX-1 might directly bind to pre-synaptic UNC-36. We did several experiments to test this idea. When co-expressed in HEK cells, GFP-tagged UNC-36 and MYC-tagged NRX-1 were co-immunoprecipitated (Fig. 4A). To determine if this interaction is conserved, we repeated these binding experiments with the corresponding mammalian proteins. Here again, we found that MYC-tagged mouse NX-1α was recovered in immunoprecipitates formed with HA-tagged α2δ-1, −2, and −3 proteins (Fig. 4B). These co-immunoprecipitation experiments suggest that NX-1α binds with highest apparent affinity to α2δ-3 (Fig. 4C). To estimate the affinity of the NX-1α/α2δ-3 complex, we used recombinant bovine NX-1α protein (btNX-1α), which is 99% identical to the mouse protein, as a competitor to interfere with co-immunoprecipitation (Fig. 4D–E). These competition experiments indicate that NX-1α binds α2δ-3 with an apparent Kd ~40 nM (Fig. 4E). By contrast, high concentrations of an unrelated protein (BSA) had no effect on co-immunoprecipitation (Fig. 4F), confirming that NX-1α binds specifically to α2δ-3.

Which NX-1α domains are required for α2δ-3 binding? The α-NX ectodomain contains six laminin-like globular repeats (LG 1–6) and three EGF-like repeats (El-3) (Fig. 5A). First, we divided the ectodomain into three fragments (Ecto1–3), finding that α2δ-3 co-immunoprecipitated with Ecto1 (LG1/E1/LG2) and 3 (LG5/E3/LG6) but failed to interact with Ecto2 (LG3/E2/LG4) (Fig. 5B). Next, we identified the domains within Ectol and 3 required for binding. The isolated LG1 and 5 domains co-immunoprecipitated with α2δ-3 while LG2 and 6 lacked binding activity (Fig. S3A–B). To confirm that these domains are

required for binding to α2δ-3, we deleted LG1 and 5 from the full length NX-1α and found that this mutant protein (ΔLG1/5) failed to bind α2δ-3 (Fig. 5C).

Having mapped the mouse NX-1α sequences required for α2δ-3 binding, we next asked if similar sequences are required for binding of the worm proteins. UNC-36 co-immunoprecipitated with the isolated LG1 domain of NRX-1 but not with the isolated LG5 domain (Fig. S3C). To confirm that binding of the worm proteins is mediated only by LG1, we constructed a mutant NRX-1 protein lacking LG1 (ΔLG1) and found that it failed to co-immunoprecipitate with UNC-36 (Fig. 5D). To determine if NRX-1 binds UNC-36 *in vivo*, we constructed transgenic animals containing FLAG-tagged NRX-1 (expressed in muscles) and GFP-tagged UNC-36 (expressed by the *unc-36* promoter). In extracts prepared from these transgenic animals, NRX-1 was detected in immunoprecipitates formed with anti-GFP antibodies but was not recovered in those formed with an unrelated antibody (anti-MYC) (Fig. 6A). These results lead to three conclusions: 1) α-NX binds α2δ with high affinity both in transfected cells and in transgenic worms; 2) this interaction is conserved across phylogeny; and 3) interaction of the mouse proteins is mediated by α-NX's LG1 and 5 domains while binding of the worm proteins only requires LG1. Because NL binds the LG6 domain (Arac et al., 2007; Fabrichny et al., 2007), α-NX could potentially bind simultaneously to NL and α2δ. Thus, trans-synaptic α-NX/NL complexes could bind α2δ subunits, providing a potential mechanism for retrograde synaptic signaling.

NLG-1 promotes NRX-1 binding to UNC-36/α2δ

Next, we asked how NLG-1 promotes retrograde signaling. Inhibition of ACh release in *mir-1* mutants is blocked in mutants lacking NLG-1 expression in motor neurons, suggesting that pre-synaptic NLG-1 somehow promotes retrograde signaling (Hu et al., 2012). NLG-1 is localized to pre-synaptic terminals and directly binds NRX-1 (Fig. S4C) (Hu et al., 2012). Based on these results, we hypothesized that NLG-1 and UNC-36/α2δ function together as co-receptors to coordinately bind post-synaptic NRX-1. We did several experiments to test this idea. First, to function as a co-receptor for NRX-1, NLG-1 must associate with UNC-2/CaV2 complexes at pre-synapses. Consistent with this idea, NLG-1 pre-synaptic enrichment was significantly reduced in both *unc-2* and *unc-36* mutants (Fig. 6C–D), as would be expected if NLG-1 is physically coupled to pre-synaptic UNC-2/CaV2. Next, we asked if *nlg-1* mutations alter UNC-36/α2δ binding to NRX-1. Consistent with this idea, the *in vivo* co-immunoprecipitation of GFP-UNC-36 and FLAG-NRX-1 was significantly reduced in *nlg-1* mutants (Fig. 6A–B), indicating that endogenously expressed NLG-1 promotes NRX-1 binding to UNC-36. Taken together, these results suggest that pre-synaptic NLG-1 orients NRX-1's ectodomain in the synaptic cleft to promote binding to UNC-36.

UNC-36/α2δ binding to NRX-1/NX α is required for retrograde inhibition

Next, we asked if NRX-1 binding to UNC-36 is required for the retrograde signal. As we previously showed, *nrx-1* null mutations block the retrograde inhibition of mEPSC rate in *mir-1* mutants. This *nrx-1* defect in retrograde inhibition is rescued by a transgene restoring NRX-1 expression to body muscles (Fig. 7A–B). By contrast, a mutant *nrx-1* transgene lacking the LG1 domain (ΔLG1) lacked rescuing activity (Fig. 7A–B), suggesting that post-synaptic NRX-1 binding to pre-synaptic UNC-36 is required for retrograde inhibition. To

confirm that the ΔLG1 protein was properly expressed, we analyzed a ΔLG1 protein containing an mCherry tag in the ectodomain (^{mCh}ΔLG1). Animals expressing ^{mCh}ΔLG1 in muscles exhibited punctate fluorescence in the nerve cord (Fig. S4A), suggesting that deleting the LG1 domain did not prevent trafficking of NRX-1 to muscle arms. To further control for its expression and function, we confirmed that ΔLG1 expressed in HEK cells binds to an NLG-1/Fc fusion protein (Fig. S4B–C). Together these experiments suggest that ΔLG1 is expressed and properly folded but is unable to mediate retrograde inhibition of ACh release.

The retrograde signal decreases UNC-36/α2δ abundance at pre-synaptic elements

Thus far, our results suggest that post-synaptic NRX-1 inhibits tonic ACh release by binding to an auxiliary subunit (UNC-36/α2δ) of pre-synaptic UNC-2/CaV2 channels. We next asked if activating the retrograde signal alters the pre-synaptic localization of UNC-36. Consistent with this idea, we found that mngUNC-36 puncta fluorescence was significantly decreased in *mir-1* mutants and that this effect was eliminated in *mir-1; nrx-1* and *mir-1; nlg-1* double mutants (where retrograde signaling is blocked) (Fig. 7C–D). By contrast, the decreased mngUNC-36 puncta intensity observed in *unc-2* mutants was not prevented by mutations inactivating the retrograde signal (Fig. S4D–E). To determine if miR-1's effects on mngUNC-36 are caused by decreased transgene expression or by a change in synaptic varicosities, we analyzed miR-1's effects on soluble mCherry (co-expressed with mngUNC-36 in the DA/DB neurons). Unlike mngUNC-36, mCherry puncta intensity was unaltered in *mir-1* mutants (Fig. S2A–B). The synaptic enrichment (ΔF/F) of mngUNC-36 (normalized to mCherry) was also significantly reduced in *mir-1* mutants (Fig. S2C). Thus, altered transgene expression and altered axonal morphology are unlikely to explain the decreased synaptic abundance of mngUNC-36 observed in *mir-1* mutants. Collectively, these results suggest that trans-synaptic NLG-1/NRX-1 complexes decrease UNC-36 localization to pre-synaptic elements, thereby inhibiting ACh release.

NX-1α inhibits CaV2.2 channel function

The preceding results suggest that NRX-1 binding to pre-synaptic UNC-36/α2δ inhibits ACh release coupled to UNC-2/CaV2. To determine if α-NX binding alters CaV2 function, we reconstituted mammalian CaV2.2 channels by co-expressing the CaV2.2 α1, β3, and α2δ-3 subunits in HEK cells. Because NX proteins are localized pre-synaptically in mammalian neurons, we tested NX's functional impact by co-expressing mouse NX-1α with CaV2.2 subunits. We found that NX-1α expression dramatically decreased calcium current density (Fig. 8A–B) without altering the voltage-dependence of CaV2.2 activation (Fig. 8C–D). This effect was not observed when we expressed a mutant NX-1α (ΔLG1/5) deficient for α2δ-3 binding (Fig. 8A–B), suggesting that α-NX binding to α2δ-3 limits the expression or function of CaV2.2. Calcium current was also unaffected when NX-1α was co-expressed with CaV2.2 channels containing either α2δ-1 or −2 subunits (Fig. S5). Thus, NX-1α can act in *cis* to limit the activity of CaV2.2, and this effect requires domains essential for α2δ binding (LG1 and 5), and is specific for channels containing α2δ-3 subunits.

NRX-1's ectodomain is cleaved by SUP-17/ADAM10

Thus far, our results suggest that worm and mammalian α-NX and α2δ proteins form a biochemical complex that regulates synaptic transmission. Although conserved, this complex has different characteristics in different species. At the *C. elegans* cholinergic NMJ, NRX-1 is post-synaptic and binds UNC-36/α2δ via its LG1 domain. In mice, NX-1α is typically pre-synaptic and binds α2δ via both LG1 and LG5. Thus, both the binding domains and synaptic orientation differ for the α-NX/α2δ complex in the two species. Despite these differences, the binding mode in worms and mammals could be similar if the *C. elegans* NRX-1 ectodomain was proteolytically cleaved from the membrane spanning domain prior to UNC-36 binding. The ectodomains of transmembrane proteins are often shed following cleavage by membrane associated proteases (Blobel, 2002; Weber and Saftig, 2012). The NL and β-NX ectodomains are both shed in mammalian neurons (Bot et al., 2011; Peixoto et al., 2012; Suzuki et al., 2012). Thus, if NRX-1 were cleaved, the shed ectodomain could bind pre-synaptic UNC-36 in an orientation similar to that exhibited by α-NX embedded in the pre-synaptic membrane.

To test this idea, we asked if NRX-1 is proteolytically processed *in vivo* (Fig. 9). For this experiment, we expressed NRX-1 containing a GFP tag in the cytoplasmic domain (NRX-1^{GFP}) in body muscles and analyzed GFP containing proteins in membrane extracts by western blotting. In wild type animals, the most abundant GFP containing protein exhibited an apparent molecular weight (~35 Kd) consistent with a carboxy-terminal fragment (CTF) cleaved in NRX-1's juxtamembrane stalk region (Fig. 9A–B). A GFP containing band of ~195 Kd (consistent with full length NRX-1^{GFP}) was faintly detected in wild type animals (Fig. 9A–B). To confirm that the NRX-1 ectodomain is shed, we expressed NRX-1 containing an mCherry tag in the ectodomain (^{mCh}NRX-1) in body muscles and analyzed fluorescence in the endolysosomal compartment of coelomocytes (Fig. 9C–D). Coelomocytes are scavenger cells that endocytose proteins secreted into the body cavity (Fares and Greenwald, 2001). Expressing ^{mCh}NRX-1 in muscles produced brightly fluorescent coelomocytes whereas expressing the cytoplasmically tagged NRX-1^{GFP} did not produce detectable coelomocyte fluorescence (Fig. 9C–D). Taken together, these results suggest that the NRX-1 ectodomain is shed from body muscles producing a soluble cleaved molecule.

Ectodomain shedding is typically mediated by membrane associated ADAM proteases. To identify the protease responsible for NRX-1 shedding, we analyzed ^{mCh}NRX-1 fluorescence in mutants lacking SUP-17/ADAM10, ADM-4/ADAM17, and MIG-17/ADMTS. Shedding was assayed by analyzing ^{mCh}NRX-1 coelomocyte fluorescence. Intact (uncleaved) NRX-1 molecules were assayed by analyzing ^{mCh}NRX-1 puncta intensity in the dorsal nerve cord. ^{mCh}NRX-1 coelomocyte fluorescence was significantly reduced in *sup-17* mutants (Fig. 9C–D), but was not obviously altered in the other two mutants (data not shown). Consistent with decreased NRX-1 shedding, ^{mCh}NRX-1 puncta fluorescence in the dorsal nerve cord was significantly increased in *sup-17* mutants (Fig. 9E–F). To confirm that SUP-17/ADAM10 is required for NRX-1 ectodomain shedding, we analyzed NRX-1^{GFP} cleavage by western blotting. In *sup-17* mutants, the abundance of the cleaved CTF^{GFP} was dramatically reduced whereas the abundance of full length NRX-1^{GFP} was significantly

increased (Fig. 9B), both consistent with decreased ectodomain cleavage. Collectively, these results suggest that a significant fraction of NRX-1 expressed in muscles is cleaved by SUP-17/ADAM10, producing a soluble ectodomain that is released into the body cavity.

NRX-1 shedding is required for retrograde synaptic inhibition

Next, we did several experiments to determine if the shed ectodomain is the active form of NRX-1 that mediates retrograde synaptic inhibition. The effects of *mir-1* mutations on tonic ACh release were blocked in *mir-1 sup-17* double mutants (Fig. 9G–H), suggesting that NRX-1 shedding is required for retrograde signaling. Next, we asked if NRX-1 shedding is enhanced during retrograde signaling. When the retrograde signal was activated (in *mir-1* mutants), ^{mCh}NRX-1 coelomocyte fluorescence was significantly increased (Fig. 9C–D) while dorsal cord ^{mCh}NRX-1 puncta fluorescence was decreased (Fig. 9E–F), both indicating increased NRX-1 shedding. The increased NRX-1 shedding observed in *mir-1* mutants was abolished in *mir-1 sup-17* double mutants, as indicated by analysis of ^{mCh}NRX-1 coelomocyte and puncta fluorescence. To further investigate the link between retrograde signaling and NRX-1 shedding, we analyzed shedding in two mutants that block retrograde signaling (*mef-2* and ΔLG1) (Fig. S6). The enhanced NRX-1 shedding exhibited by *mir-1* mutants was blocked in *mir-1; mef-2* double mutants (Fig. S6), which could account for MEF-2's effect on retrograde signaling (Hu et al., 2012; Simon et al., 2008). By contrast, deleting NRX-1's LG1 domain had no apparent effect on coelomocyte fluorescence (Fig. S6). Thus, NRX-1 shedding does not require binding to UNC-36. This result also suggests that deleting the LG1 domain does not prevent NRX-1 delivery to the cell surface nor cleavage by SUP-17/ADAM10. Collectively, these results support the idea that the shed ectodomain is the active form of NRX-1 for retrograde signaling, and that miR-1 and MEF-2 regulate NRX-1 shedding.

Discussion

Our results lead to seven principal conclusions. First, tonic and evoked ACh release at the *C. elegans* body wall NMJ are mediated by distinct classes of CaV channels. Second, UNC-36/α2δ is an essential auxiliary subunit for UNC-2/CaV2 but is not required for the function of EGL-19/CaV1. Third, in *mir-1* mutants, trans-synaptic NLG-1/NRX-1 complexes selectively inhibit release coupled to UNC-2/CaV2 but not that coupled to EGL-19/CaV1. Fourth, worm and rodent α-NX proteins bind with high affinity to α2δ proteins. Fifth, retrograde synaptic inhibition at the *C. elegans* NMJ is mediated by post-synaptic NRX-1 binding to pre-synaptic UNC-36/α2δ. Sixth, α-NX binding to α2δ-3 inhibits the function of mammalian CaV2.2 channels. And seventh, NRX-1 is cleaved by SUP-17/ADAM10 and the shed ectodomain mediates retrograde synaptic inhibition. Collectively, these results identify a conserved biochemical mechanism to explain how trans-synaptic α-NX-NL complexes regulate presynaptic function. Below we discuss the significance of these findings.

Different CaVs for evoked and tonic release

Prior studies showed that spontaneous and evoked release are mediated by distinct pools of SVs (Sara et al., 2005) and is regulated by distinct sets of synaptic proteins (DiAntonio and

Schwarz, 1994; Groffen et al., 2011; Hobson et al., 2011; Hu et al., 2015; Littleton et al., 1994; Martin et al., 2011; Pang et al., 2011; Pang et al., 2006). Here we show that different CaVs mediate tonic and evoked responses. Evoked EPSCs are nearly completely mediated by SVs coupled to UNC-2/CaV2 whereas tonic release comprises a mixture of UNC-2 and EGL-19/CaV1 coupled SVs. Although EGL-19/CaV1 coupled SVs account for roughly half of tonic release, it is intriguing that only UNC-2/CaV2 coupled SVs participate in evoked responses.

What accounts for the failure of EGL-19/CaV1 coupled SVs to participate in evoked responses? This discrepancy could reflect differences in the coupling of motor neuron depolarization to calcium entry through UNC-2/CaV2 and EGL-19/CaV1. For example, if EGL-19/CaV1 activates at more positive membrane potentials than UNC-2/CaV2, direct stimulation of motor neuron cell bodies may not efficiently activate synaptic EGL-19. In this scenario, fusion of EGL-19/CaV1 coupled SVs would contribute more prominently to responses produced by inputs that more extensively depolarize nerve terminals.

α-NX proteins are directly coupled to CaV2 by binding to α2δ

Prior studies showed that mouse neurons lacking all α-NX proteins have dramatically reduced presynaptic CaV2 current and a corresponding decrease in synaptic transmission (Missler et al., 2003). Based on these findings, it has long been proposed that α-NX proteins are biochemically connected in some manner to CaV2. Our results suggest that α-NXs are coupled to CaV2 by their direct binding to α2δ subunits. Mammalian NX-1α binds directly to α2δ-1, 2, and 3 with high affinity and that this interaction is conserved between the corresponding *C. elegans* proteins (UNC-36/α2δ and NRX-1). However, co-expression of NX-1α with CaV2.2 channels in HEK cells did not produce a general enhancement of calcium currents. Instead, NX-1α expression significantly inhibited calcium currents formed by channels containing α2δ-3 subunits.

Our results suggest that trans-synaptic NX-NL complexes form a physical bridge linking release sites to clustered post-synaptic receptors. We find that NX-NL complexes associate with the pre-synaptic CaV2 channels that drive neurotransmitter release. Prior studies showed that NX-NL complexes immobilize receptor clusters at post-synapses (Aoto et al., 2013; Heine et al., 2008; Kang et al., 2008; Nam and Chen, 2005; Tong et al., 2015). A recent study showed that pre-synaptic α2δ2 promotes post-synaptic accumulation of GluA4 receptors at mouse inner hair cell synapses (Fell et al., 2016), providing further support for a direct link between release sites and post-synaptic receptors. Direct coupling of release sites to post-synaptic receptors could play several important roles in synaptic transmission. Coupling would be expected to shorten the latency between the presynaptic action potential and activation of post-synaptic currents (Sabatini and Regehr, 1996). Coupling would optimally localize clustered receptors within the post-synaptic density so that they could be efficiently activated by synaptic vesicle fusion (Franks et al., 2003). And coupling would decrease the frequency of post-synaptic failures.

Several studies proposed that α2δ subunits can promote synapse formation. α2δ-1 promotes excitatory synapse formation in cultured rat retinal ganglion cells (Eroglu et al., 2009). In this case, thrombospondin was implicated as the α2δ-1 ligand responsible for the

synaptogenic activity. *Drosophila* mutants lacking α2δ also exhibit decreased synapse formation; however, in this case, the ligand responsible for this effect was not identified (Kurshan et al., 2009). Our results suggest that α2δ proteins could promote synapse formation (or maturation) via their ability to bind α-NX proteins, which also exhibit synaptogenic activity (Graf et al., 2004; Nam and Chen, 2005).

A new mechanism for post-synaptic regulation of presynaptic release

Many studies have shown that post-synaptic cells have the capacity to alter presynaptic properties via retrograde synaptic signals. In some cases, production and release of retrograde signals are elicited by changes in the activity of post-synaptic cells. Examples of activity-induced retrograde signals include BDNF, nitric oxide, and endocannabinoids (Regehr et al., 2009). In other cases, the identity of the post-synaptic cell dictates a stable change in pre-synaptic properties. In layer 2/3 of the rat somatosensory cortex, pyramidal neurons provide direct synaptic input to Somatostatin (SOM) expressing and Parvalbumin (PV) expressing interneurons. Pyramid-SOM synapses exhibit low release probability and short term facilitation while the Pyramid-PV synapses have high release probability and are depressing (Koester and Johnston, 2005; Reyes et al., 1998). A similar example was also described in crickets (Davis and Murphey, 1993). Thus, divergent outputs from a single presynaptic cell can exhibit significantly different release probabilities and plasticity depending on the identity of the post-synaptic cell.

The molecular basis for these post-synaptic effects was identified in one case. In the mouse hippocampus, a post-synaptic protein (Elfn1) increases release probability at Pyramidal-interneuron synapses (Sylwestrak and Ghosh, 2012). Our results suggest that the binding of trans-synaptic NX-NL complexes to presynaptic α2δ subunits provides a second potential mechanism for post-synaptic cells to alter presynaptic release and plasticity. α-NX proteins have multiple binding partners, including LRRTM2 (de Wit et al., 2009; Ko et al., 2009), calsyntenin (Pettem et al., 2013), cerebellin (Uemura et al., 2010), and neurexophilin (Missler et al., 1998). We propose that different forms of retrograde signaling could be mediated by this diverse set of α-NX binding partners. Our results also suggest that these trans-synaptic adhesive complexes will have different effects at synapses utilizing α2δ-1, 2, or 3 subunits.

A new role for α-NX ectodomain shedding

We showed that SUP-17/ADAM10 cleaves NRX-1 and that the shed ectodomain binds pre-synaptic UNC-36/α2δ, thereby inhibiting ACh release. Although *sup-17* mutations block retrograde signaling, our results do not exclude the idea that other proteases also play a role (accounting for the residual NRX-1 shedding in *sup-17* mutants). Our results also do not exclude the idea that other SUP-17 substrates (in addition to NRX-1) also play a role in retrograde signaling. Interestingly, ADAM10 cleaves NL in mammalian neurons (Suzuki et al., 2012). The shed NL ectodomain inhibits neurotransmitter release at mammalian synapses (Peixoto et al., 2012); however, the mechanism for this effect has not been determined. Thus, in both worms and mammals, a post-synaptic protease (SUP-17/ADAM10) induces shedding of a post-synaptic adhesion molecule (NL in mammals, NX in worms), thereby inhibiting neurotransmitter release. Because NRX-1 function in retrograde

signaling is mediated by the shed ectodomain, it could bind pre-synaptic UNC-36/α2δ in an orientation similar to that exhibited by α-NX proteins embedded in the pre-synaptic membrane. Thus, although the synaptic polarity of NX and NL may differ between synapses, reversed polarity does not require distinct biochemical functions for these complexes.

Identifying shed NRX-1 as the active mediator provides several insights into the mechanisms controlling retrograde signaling at this synapse. Although retrograde inhibition is induced by inactivating the muscle microRNA miR-1, prior studies did not provide a direct link between miR-1 and NRX-1. Here we show that mutations inactivating SUP-17/ADAM10 block the retrograde signal and the enhanced NRX-1 shedding in *mir-1* mutants. The *sup-17* mRNA is a predicted miR-1 target (www.targetscan.org), which could explain how miR-1 alters NRX-1 function in muscle. Retrograde signaling is also blocked by *mef-2* mutations (Hu et al., 2012; Simon et al., 2008); however, *nrx-1* is not a direct MEF-2 target. Here we show that *mef-2* mutations prevent the enhanced NRX-1 shedding observed in *mir-1* mutants, suggesting that a MEF-2 target promotes NRX-1 shedding in some manner. These results also suggest that regulation of ectodomain shedding could help explain Mef2's effects on synapse stability in mammalian neurons (Flavell et al., 2006). Although pre-synaptic NLG-1 is required for retrograde signaling, our prior studies had not defined how NLG-1 is linked to altered ACh release. Here we show that NLG-1 is associated with pre-synaptic UNC-2/CaV2, where it promotes NRX-1 binding to UNC-36/α2δ. Because the active mediator is the proteolytically shed NRX-1 ectodomain, efficient binding to UNC-36 may require the presence of NLG-1 as a co-receptor. Thus, identifying shed NRX-1 as the active mediator has significantly improved our understanding of how retrograde signaling operates at this synapse.

Implications for understanding Autism

Recurrent de novo mutations in NX, NL, CACNA2D3 (which encodes α2δ-3), and Mef2c have been shown to confer risk for Autism spectrum disorders (ASDs) (De Rubeis et al., 2014; Iossifov et al., 2012; Neale et al., 2012; Novara et al., 2010). Because these molecules all function together to mediate retrograde regulation of presynaptic function, our results provide further support for the idea that defects in retrograde synaptic signals could play an important role in the pathophysiology of ASD (Hu et al., 2012). In this regard, it is intriguing that CACNA2D3 mutations but not CACNA2D1 or 2 mutations have been found in ASD, implying that altered α2δ-3 is selectively important for ASD. This selectivity for CACNA2D3 mutations in ASD mirrors our results whereby α-NX inhibited calcium currents only when CaV2.2 was reconstituted with α2δ-3, having no effect on channels containing α2δ-1 and −2. These results support the idea that changes in α-NX binding to α2δ-3 could be particularly important in some forms of ASD.

How might changes in retrograde signaling contribute to the cognitive and developmental defects observed in ASD? Our results suggest that α-NX binding to α2δ-3 provides a mechanism for retrograde regulation of presynaptic release and plasticity. Changes in short term plasticity (i.e. facilitation versus depression) provides a mechanism to control the timing of post-synaptic cell activation. In general, depressing inputs are optimized to rapidly

activate target cells during low frequency stimulation while facilitating inputs typically activate targets later and are tuned to higher frequency stimuli (Abbott and Regehr, 2004). Thus, by regulating release probability, α-NX binding to α2δ-3 is likely to alter the timing of post-synaptic responses in cortical circuits. If NX, NL, and CACNA2D3 mutations alter release probability at excitatory-interneuron synapses, the timing of synaptic inhibition would be disrupted, which could contribute to the changes in inhibitory transmission observed in several forms of ASD (Dani et al., 2005; Rubenstein and Merzenich, 2003).

STAR METHODS TEXT

CONTACT FOR REAGENT AND RESOURCE SHARING

Further information and requests for resources and reagents should be directed to and will be fulfilled by the Lead Contact Joshua Kaplan (kaplan@molbio.mgh.harvard.edu).

EXPERIMENTAL MODEL AND SUBJECT DETAILS

***C. elegans* strains—**Strains were maintained at 20 °C under standard conditions, unless otherwise noted. OP50 *E. coli* was used as a food source for all experiments except electrophysiology where HB101 *E. coli* was utilized. Adult hermaphrodites were utilized for all experiments. A description of all alleles can be found at www.wormbase.org. Transgenic animals were prepared by micro injection, and integrated transgenes were isolated following UV irradiation.

Cell Lines—HEK293.ETN (ATCC) was obtained from Brian Seed (CCIB, MGH). HEK293.ETN and tsA201 cells were grown at 37°C, 5% CO_2. Cells were transfected by using TransFectin (BioRAD). Sf9 cells were grown in suspension in CCM-3 medium at 27°C in an air incubator with a cooling coil and shaken at 100rpm. Neither HEK293.ETN nor tsA201 cells were authenticated.

METHOD DETAILS

Antibodies—Antibodies were purchased from the vendors indicated above (see Key Resource Table) and were used as follows: mouse anti-GFP (1:1,000 for WB), mouse anti-HA (1:1,000 for WB), mouse anti-Myc (1:1,000 for WB), mouse anti-Flag (1:1,000 for WB), mouse anti-HA agarose (40 μl of 1:1 suspension for IP), mouse anti-Flag agarose (40 μl of 1:1 suspension for IP), rabbit anti-GFP Sepharose (20 μl of 1:1 suspension for IP), rabbit anti-Myc Agarose (40 μl of 1:1 suspension for IP).

Plasmids—All worm expression vectors are modified versions of pPD49.26 (A. Fire). Standard methods were utilized to construct all plasmids. A 3kb *myo-3* myosin promoter was used for expression in body muscles, a 2.6 kb *unc-129* promoter was used for expression in DA and DB motor neurons. NRX-1a (C29A12.4a), and UNC-36 (C50C3.9a) cDNAs were amplified from a cDNA library using gene specific primers. Mouse NX-1a cDNA was provided by T. Sudhof (Stanford). Rat α2δ1, mouse α2δ2 and mouse α2δ3 cDNAs were provided by A. Dolphin (UCL). *nuIs553* contains an mNeonGreen (mng) tagged UNC-36 construct (mng inserted immediately after signal peptide). *nuIs502* contains sfGFP tagged UNC-36 and FLAG (2 copies) tagged NRX-1 constructs, where both tags

were inserted immediately after the signal peptide. *nuIs499* contains mCherry tagged NRX-1 where mCherry was inserted in frame immediately after the signal peptide. *nuls449* contains sfGFP tagged NLG-1 (tag inserted in the cytoplasmic tail 20 amino acids prior to the carboxy-terminus). The sfGFP-UNC-36/pcDNA3.1 construct (KP#2444) contains sfGFP-UNC-36 in pCDNA3.1 (sfGFP inserted after the signal peptide). Full length and chimeric NRX-1 constructs (KP#3241) contain the MYC tag (inserted after signal peptide) in pCMV.

Recombinant Cow NX-1α purification—pFastBac btNrx-1 L1-L6 his6 was a generous gift from G. Rudenko. We generated and amplified the baculovirus in Sf9 cells according to standard procedures, and protein purification was carried out as described (Chen et al., 2011) with minor modifications. Briefly, Sf9 cells were infected with baculovirus and allowed to secrete protein in the medium for 90hrs; supernatants were pooled, concentrated and adjusted to 500mM NaCl; pH was adjusted to 7.2, then the supernatant was pumped over a HisTrap Excel column. After several washes (20mM HEPES pH 7.5 + 500mM NaCl and 20mM HEPES pH 7.5 + 150mM NaCl), btNrx-1 his6 was eluted with 20mM HEPES / 150mM NaCl /250mM imidazole pH 7.5 (10 column volumes). After dialysis into 20mM HEPES pH 7.5 + 50mM NaCl, the protein was further purified on a MonoQ column using a 50mM-1M NaCl gradient. Positive fractions were pooled, concentrated and applied to a Superdex200 16/600 column and eluted with PBS; positive fractions were pooled, concentrated and used fresh for experiments. The bovine Nrx-1 L1-L6 thus purified was free of contaminants (as judged by Coomassie staining).

Electrophysiology—Electrophysiology was done on dissected *C. elegans* adults as previously described (Hu et al., 2013). Worms were superfused in an extracellular solution containing 127 mM NaCl, 5 mM KC1, 26 mM $NaHCO_3$, 1.25 mM NaH_2PO_4, 20 mM glucose, l mM $CaCl_2$ and 4 mM $MgCl_2$, bubbled with 5% CO_2, 95% O_2 at 20°C. Whole cell recordings were carried out at −60 mV using an internal solution containing 105 mM $CSCH_3SO_3$, 10 mM CsCl, 15 mM CsF, 4 mM $MgCl_2$, 5mM EGTA, 0.25 mM $CaCl_2$, 10 mM HEPES and 4 mM Na_2ATP, adjusted to pH 7.2 using CsOH. Under these conditions, we only observed cholinergic mEPSCs. Stimulus-evoked EPSCs were evoked by placing a borosilicate pipette (5–10 μm) near the ventral nerve cord (one muscle distance from the recording pipette) and applying a 0.4 ms, 85 μA square pulse using a stimulus current generator (WPI). Statistical significance was determined using a two-tailed Student's t-test. Currents mediated by EGL-19/CaV1 channels in body muscles were recorded by depolarizing the membrane potential from −60mV to +10mV. For analysis of calcium currents, the extracellular solution contained 140 mM TEA-C1, 5 mM $CaCl_2$, 1 mM $MgCl_2$, 3 mM 4-aminopyridine, 10 mM glucose, 5 mM sucrose, and 15 mM HEPES (pH 7.4 adjusted by CsOH, 330 mOsm). The pipette solution consisted of 140 mM CsCl, 10 mM TEA-C1, 5 mM $MgCl_2$, 5 mM EGTA, and 10 mM HEPES (pH 7.2 adjusted by CsOH, 320 mOsm) (Gao and Zhen, 2011). The EGL-19/CaV1 current was completely blocked by bath application of 10 μM Nemadipine-A.

Microscopy—For imaging studies, images were captured using a 60x objective (NA 1.45) on an Olympus FV-1000 confocal microscope at 5x digital zoom. Worms were immobilized

with 0.1μm polystyrene microspheres (Polysciences), and pads composed of 10% agarose in M9 salts. Maximum intensity projections of Z-series stacks were made using Metamorph 7.1 software (Universal Imaging). Line scans of dorsal cord fluorescence were analyzed in an automated manner using Igor Pro (WaveMetrics). Mean fluorescence of Reference Slides, which was measured during each experiment, was used to control for changes in illumination intensity. All fluorescence values are normalized to wild type controls to facilitate comparison. To assess synaptic accumulation of fluorescent proteins, we measured $\Delta F/F = F_{puncta}\text{-}F_{axon}/F_{axon}$. Statistical significance was determined by oneway ANOVA or student t-tests.

Co-Immunoprecipitation—All tagged protein constructs were transfected or co-transfected into HEK293.ETN cells using the TransFectin reagent (Biorad), and cells were harvested 60 hours post-transfection.

Membrane extracts were prepared from transfected HEK cells as described (Eroglu et al., 2009). Briefly, cells were pelleted and re-suspended in ice-cold hypotonic buffer (10mM Tris pH 7.4, 1mM $CaCl_2$ and 1mM $MgCl_2$and protease inhibitors), and incubated on ice for 15 minutes. Washed cells were disrupted by using a dounce homogenizer. The nuclei and unbroken cells were removed by centrifugation (5 minutes, 300g). The membranes were isolated from the post-nuclear supernatant by centrifugation (20 minutes, 20,000g). The membranes were solubilized in RIPA buffer (20mM HEPES PH7.4, 150mM NaCl, 2mM $MgCl_2$, 0,1mM EDTA, 1% Triton and proteinase inhibitors) and insoluble debris was removed by centrifugation (20 minutes, 20,000g). The resulting membrane extracts were incubated with agarose or sepharose beads conjugated to anti-HA (Sigma-Aldrich) or anti-GFP antibodies overnight at 4°C while rotating. Bound proteins were eluted with sample buffer and loaded on gradient SDS-PAGE gels (4–12% or 3–8%, Invitrogen).

Worm Co-Immunoprecipitation—Extracts were prepared from young adult worms expressing sfGFP-UNC-36 and Flag-NRX-1 using a microfluidizer in buffer A (50 mM HEPES PH7.7, 50 mM KAc, 2mMgAc2, 250 mM sucrose, 1 mM EDTA and proteinase inhibitors). Worm extracts were clarified by centrifugation (12 min, 7000g, 4°C). Membranes were isolated from the resulting supernatant by ultracentrifugation (40 min, 45,000g). Membrane proteins were solubilized with a dounce homogenizer (5 times) in IP buffer (20 mM HEPES PH7.4, 150 mMNaCl, 2 mM$MgCl_2$, 0,1 mMEDTA, 1% Triton and proteinase inhibitors), and insoluble debris was removed by centrifugation (10 minutes, 20,000g). The resulting membrane extracts were incubated with anti-GFP sepharose beads overnight at 4°, the beads were washed three times with IP buffer, and bound proteins were eluted with loading buffer.

Fc pull down assays—NLG-1/Fc fusion protein constructs were transfected into 293.ETN cells using the Transfectin reagent (Biorad), conditioned medium was harvested 72 hours post-transfection, and Fc proteins were purified with protein A- sepharose beads.

293.ETN cells transfected with NRX- 1 or NRX-1ΔLG1 were subjected to membrane prep, and membrane proteins were solubilized with RIPA buffer (HEPES/KOH PH7.4, 0. 1mM EDTA, 1% Triton, 2mM $CaCl_2$, $MgCl_2$ with protease inhibitors). Cell debris was removed

by centrifugation (20 minutes, 10,000g). Membrane extracts were incubated overnight (at 4 °C) with protein A-Sepharose bound to Fc or NLG-1/Fc. Beads were washed three times with RIPA buffer, re-suspended in sample buffer, and eluted proteins were analyzed by Western blot.

Rat CaV2.2 recordings—We used the human tsA201 cell line to assess calcium currents expressed with different combinations of subunits. TsA201 cells were transfected at 70–80 % confluence with cDNA plasmids encoding $Ca_V2.2$ (#AF055477), $Ca_V\beta_3$ (#M88751), and one of $Ca_V\alpha_2\delta_1$-HA (KP#2097), $Ca_V\alpha_2\delta_2$-HA (KP#2098), or $Ca_V\alpha_2\delta_3$-HA (KP#2099) with or without mouse NX-1α [WT (KP#3241) or ΔLG1/5 (KP#3265)] or empty vector pcDNA3.1 at 1:1:1:1 molar ratio using Lipofectamine 2000 (Invitrogen). Enhanced green fluorescent protein cDNA (eGFP; BD Bioscience) was included in the transfection mix to detect transfected cells. Cells were cultured in DMEM supplemented with 10% FBS.

Whole-cell $Ca_V2.2$ currents in tsA201 cells were recorded by patch clamp 24 h post-transfection. Recordings from cells expressing different combinations of subunits were interleaved each day, by an experimenter unaware of the identity of the transfected constructs in each experiment. For each combination of expression vectors, we recorded currents from cells from 8 independent transfections using Axopatch 200B amplifier (Molecular Devices, LLC). Currents were filtered at 5 kHz (-3 dB) and sampled at 50 kHz (Digidata 1440A; Molecular Devices). Recording pipettes were filled with an internal solution containing (in mM): 126 CsCl, 10 EGTA, 1 EDTA, 10 HEPES, 4 Mg-ATP, pH 7.2 with CsOH and had resistance of 2–4 MΩ. Series resistances were < 5 MΩ and compensated to −80% with a 10 μs lag-time. External solution contained (in mM): 1 $CaCl_2$, 4 $MgCl_2$, 10 HEPES, 135 choline chloride, pH adjusted to 7.2 with CsOH. Macroscopic $Ca_V2.2$ currents were evoked by 35 ms voltage steps applied from a holding potential of-100 mV. Leak currents were subtracted online using P/-4 protocol. All recordings were made at room temperature.

QUANTITATION AND STATISTICAL ANALYSIS

Quantitation and statistical details can be found in the figure legends or Method Details section. All data are reported as mean ± s.e.m. Statistical significance between means was calculated ONE-way ANOVA or student t-tests. *p < 0.05; **p < 0.01; *** p < 0.001. Sample sizes are reported and defined in each figure. For *C. elegans* imaging experiments, sample sizes refer to the number of animals analyzed for each genotype. For *C. elegans* electrophysiology experiments, sample size refers to the number of muscle cell recordings for each genotype. For co-immunoprecipitation experiments, sample sizes refer to the number of independent replicate experiments.

Supplementary Material

Refer to Web version on PubMed Central for supplementary material.

Acknowledgments

We thank the following for strains and reagents: the *C. elegans* Genetics Stock Center, Brian Seed, Gabby Rudenko, Annette Dolphin, Tim Ryan, and Tom Sudhof. We thank members of the Kaplan, Hu, and Lipscombe labs for

helpful discussions and critical comments on the manuscript. This work was supported by research grants to JK (NIH NS32196; NIH GM54728; Simons Foundation SF273555), DL (NIH NS55251), and ZH (ARC, DP160100849). DN was supported by a fellowship from the Autism Science Foundation (REG 15-006).

References

Abbott LF, Regehr WG. Synaptic computation. Nature. 2004; 431:796–803. [PubMed: 15483601]

Aoto I, Martinelh DC, Malenka RC, Tabuchi K, Sudhof TC. Presynaptic neurexin-3 alternative splicing trans-synaptically controls postsynaptic AMPA receptor trafficking. Cell. 2013; 154:75–88. [PubMed: 23827676]

Arac D, Boucard AA, Ozkan E, Strop P, Newell E, Sudhof TC, Brunger AT. Structures of neuroligin-1 and the neuroligin-1/neurexin-1 beta complex reveal specific protein-protein and protein-Ca2+ interactions. Neuron. 2007; 56:992–1003. [PubMed: 18093522]

Bernstein GM, Jones OT. Kinetics of internalization and degradation of N-type voltage-gated calcium channels: role of the alpha2/delta subunit. Cell Calcium. 2007; 41:27–40. [PubMed: 16759698]

Blobel CP. Functional and biochemical characterization of ADAMs and their predicted role in protein ectodomain shedding. Inflamm Res. 2002; 51:83–84. [PubMed: 11926318]

Bot N, Schweizer C, Ben Halima S, Fraering PC. Processing of the synaptic cell adhesion molecule neurexin-3beta by Alzheimer disease alpha- and gamma-secretases. J Biol Chem. 2011; 286:2762–2773. [PubMed: 21084300]

Canti C, Nieto-Rostro M, Foucault I, Heblich F, Wratten J, Richards MW, Hendrich J, Douglas L, Page KM, Davies A, et al. The metal-ion-dependent adhesion site in the Von Willebrand factor-A domain of alpha2delta subunits is key to trafficking voltage-gated Ca2+ channels. Proc Natl Acad Sci U S A. 2005; 102:11230–11235. [PubMed: 16061813]

Chen F, Venugopal V, Murray B, Rudenko G. The structure of neurexin 1alpha reveals features promoting a role as synaptic organizer. Structure. 2011; 19:779–789. [PubMed: 21620716]

Chen K, Gracheva EO, Yu SC, Sheng Q, Richmond J, Featherstone DE. Neurexin in embryonic Drosophila neuromuscular junctions. PLoS One. 2010; 5:e11115. [PubMed: 20559439]

Dani VS, Chang Q, Maffei A, Turrigiano GG, Jaenisch R, Nelson SB. Reduced cortical activity due to a shift in the balance between excitation and inhibition in a mouse model of Rett syndrome. Proc Natl Acad Sci U S A. 2005; 102:12560–12565. [PubMed: 16116096]

Davis GW, Murphey RK. A role for postsynaptic neurons in determining presynaptic release properties in the cricket CNS: evidence for retrograde control of facilitation. J Neurosci. 1993; 13:3827–3838. [PubMed: 8366348]

De Rubeis S, He X, Goldberg AP, Poultney CS, Samocha K, Cicek AE, Kou Y, Liu L, Fromer M, Walker S, et al. Synaptic, transcriptional and chromatin genes disrupted in autism. Nature. 2014; 515:209–215. [PubMed: 25363760]

de Wit J, Sylwestrak E, O'Sullivan ML, Otto S, Tiglio K, Savas JN, Yates JR 3rd, Comoletti D, Taylor P, Ghosh A. LRRTM2 interacts with Neurexin1 and regulates excitatory synapse formation. Neuron. 2009; 64:799–806. [PubMed: 20064388]

Dean C, Scholl FG, Choih J, DeMaria S, Berger J, Isacoff E, Scheiffele P. Neurexin mediates the assembly of presynaptic terminals. Nat Neurosci. 2003; 6:708–716. [PubMed: 12796785]

DiAntonio A, Schwarz T. The effect on synaptic physiology of synaptotagmin mutations in Drosophila. Neuron. 1994; 12:909–920. [PubMed: 7909234]

Dolphin AC, Wyatt CN, Richards J, Beattie RE, Craig P, Lee JH, Cribbs LL, Volsen SG, Perez-Reyes E. The effect of alpha2-delta and other accessory subunits on expression and properties of the calcium channel alpha1G. J Physiol. 1999; 519(Pt 1):35–45. [PubMed: 10432337]

Eroglu C, Allen NJ, Susman MW, O'Rourke NA, Park CY, Ozkan E, Chakraborty C, Mulinyawe SB, Annis DS, Huberman AD, et al. Gabapentin receptor alpha2delta-1 is a neuronal thrombospondin receptor responsible for excitatory CNS synaptogenesis. Cell. 2009; 139:380–392. [PubMed: 19818485]

Fabrichny IP, Leone P, Sulzenbacher G, Comoletti D, Miller MT, Taylor P, Bourne Y, Marchot P. Structural analysis of the synaptic protein neuroligin and its beta-neurexin complex: determinants for folding and cell adhesion. Neuron. 2007; 56:979–991. [PubMed: 18093521]

Fares H, Greenwald I. Genetic analysis of endocytosis in Caenorhabditis elegans: coelomocyte uptake defective mutants. Genetics. 2001; 159:133–145. [PubMed: 11560892]

Feinberg EH, Vanhoven MK, Bendesky A, Wang G, Fetter RD, Shen K, Bargmann CI. GFP Reconstitution Across Synaptic Partners (GRASP) defines cell contacts and synapses in living nervous systems. Neuron. 2008; 57:353–363. [PubMed: 18255029]

Felix R, Gurnett CA, De Waard M, Campbell KP. Dissection of functional domains of the voltage-dependent Ca2+ channel alpha2delta subunit. J Neurosci. 1997; 17:6884–6891. [PubMed: 9278523]

Fell B, Eckrich S, Blum K, Eckrich T, Hecker D, Obermair GJ, Munkner S, Flockerzi V, Schick B, Engel J. alpha2delta2 Controls the Function and Trans-Synaptic Coupling of Cav1.3 Channels in Mouse Inner Hair Cells and Is Essential for Normal Hearing. J Neurosci. 2016; 36:11024–11036. [PubMed: 27798183]

Flavell SW, Cowan CW, Kim TK, Greer PL, Lin Y, Paradis S, Griffith EC, Hu LS, Chen C, Greenberg ME. Activity-dependent regulation of MEF2 transcription factors suppresses excitatory synapse number. Science. 2006; 311:1008–1012. [PubMed: 16484497]

Franks KM, Stevens CF, Sejnowski TJ. Independent sources of quantal variability at single glutamatergic synapses. J Neurosci. 2003; 23:3186–3195. [PubMed: 12716926]

Futai K, Kim MJ, Hashikawa T, Scheiffele P, Sheng M, Hayashi Y. Retrograde modulation of presynaptic release probability through signaling mediated by PSD-95-neuroligin. Nat Neurosci. 2007; 10:186–195. [PubMed: 17237775]

Gao S, Zhen M. Action potentials drive body wall muscle contractions in Caenorhabditis elegans. Proc Natl Acad Sci U S A. 2011; 108:2557–2562. [PubMed: 21248227]

Graf ER, Valakh V, Wright CM, Wu C, Liu Z, Zhang YQ, DiAntonio A. RIM promotes calcium channel accumulation at active zones of the Drosophila neuromuscular junction. J Neurosci. 2012; 32:16586–16596. [PubMed: 23175814]

Graf ER, Zhang X, Jin SX, Linhoff MW, Craig AM. Neurexins induce differentiation of GABA and glutamate postsynaptic specializations via neuroligins. Cell. 2004; 119:1013–1026. [PubMed: 15620359]

Groffen AJ, Martens S, Diez Arazola R, Cornelisse LN, Lozovaya N, de Jong AP, Goriounova NA, Habets RL, Takai Y, Borst JG, et al. Doc2b is a high-affinity Ca2+ sensor for spontaneous neurotransmitter release. Science. 2011; 327:1614–1618.

Heine M, Thoumine O, Mondin M, Tessier B, Giannone G, Choquet D. Activity-independent and subunit-specific recruitment of functional AMPA receptors at neurexin/neuroligin contacts. Proc Natl Acad Sci U S A. 2008; 105:20947–20952. [PubMed: 19098102]

Hobson RJ, Liu Q, Watanabe S, Jorgensen EM. Complexin maintains vesicles in the primed state in C. elegans. Curr Biol. 2011; 21:106–113. [PubMed: 21215631]

Hoppa MB, Lana B, Margas W, Dolphin AC, Ryan TA. alpha2delta expression sets presynaptic calcium channel abundance and release probability. Nature. 2012; 486:122–125. [PubMed: 22678293]

Hu Z, Hom S, Kudze T, Tong XJ, Choi S, Aramuni G, Zhang W, Kaplan JM. Neurexin and neuroligin mediate retrograde synaptic inhibition in C. elegans. Science. 2012; 337:980–984. [PubMed: 22859820]

Hu Z, Tong XJ, Kaplan JM. UNC-13L, UNC-13S, and Tomosyn form a protein code for fast and slow neurotransmitter release in Caenorhabditis elegans. eLife. 2013; 2:e00967. [PubMed: 23951547]

Hu Z, Vashlishan-Murray AB, Kaplan JM. NLP-12 Engages Different UNC-13 Proteins to Potentiate Tonic and Evoked Release. J Neurosci. 2015; 35:1038–1042. [PubMed: 25609620]

Hunter JW, Mullen GP, McManus JR, Heatherly JM, Duke A, Rand JB. Neuroligin-deficient mutants of C. elegans have sensory processing deficits and are hypersensitive to oxidative stress and mercury toxicity. Dis Model Mech. 2010; 3:366–376. [PubMed: 20083577]

Iossifov I, Ronemus M, Levy D, Wang Z, Hakker I, Rosenbaum J, Yamrom B, Lee YH, Narzisi G, Leotta A, et al. De novo gene disruptions in children on the autistic spectrum. Neuron. 2012; 74:285–299. [PubMed: 22542183]

Kaeser PS, Deng L, Wang Y, Dulubova I, Liu X, Rizo J, Sudhof TC. RIM proteins tether Ca2+ channels to presynaptic active zones via a direct PDZ-domain interaction. Cell. 2011; 144:282–295. [PubMed: 21241895]

Kang Y, Zhang X, Dobie F, Wu H, Craig AM. Induction of GABAergic postsynaptic differentiation by alpha-neurexins. J Biol Chem. 2008; 283:2323–2334. [PubMed: 18006501]

Kattenstroth G, Tantalaki E, Sudhof TC, Gottmann K, Missler M. Postsynaptic N-methyl-D-aspartate receptor function requires alpha-neurexins. Proc Natl Acad Sci U S A. 2004; 101:2607–2612. [PubMed: 14983056]

Klugbauer N, Lacinova L, Marais E, Hobom M, Hofmann F. Molecular diversity of the calcium channel alpha2delta subunit. J Neurosci. 1999; 19:684–691. [PubMed: 9880589]

Ko J, Fuccillo MV, Malenka RC, Sudhof TC. LRRTM2 functions as a neurexin ligand in promoting excitatory synapse formation. Neuron. 2009; 64:791–798. [PubMed: 20064387]

Koester HJ, Johnston D. Target cell-dependent normalization of transmitter release at neocortical synapses. Science. 2005; 308:863–866. [PubMed: 15774725]

Kurshan PT, Oztan A, Schwarz TL. Presynaptic alpha2delta-3 is required for synaptic morphogenesis independent of its Ca2+-channel functions. Nat Neurosci. 2009; 12:1415–1423. [PubMed: 19820706]

Kwok TC, Ricker N, Fraser R, Chan AW, Burns A, Stanley EF, McCourt P, Cutler SR, Roy PJ. A small-molecule screen in C. elegans yields a new calcium channel antagonist. Nature. 2006; 441:91–95. [PubMed: 16672971]

Laine V, Frokjaer-Jensen C, Couchoux H, Jospin M. The alpha1 subunit EGL-19, the alpha2/delta subunit UNC-36, and the beta subunit CCB-1 underlie voltage-dependent calcium currents in Caenorhabditis elegans striated muscle. J Biol Chem. 2011; 286:36180–36187. [PubMed: 21878625]

Littleton JT, Stern M, Perin M, Bellen HJ. Calcium dependence of neurotransmitter release and rate of spontaneous vesicle fusions are altered in Drosophila synaptotagmin mutants. Proc Natl Acad Sci U S A. 1994; 91:10888–10892. [PubMed: 7971978]

Liu Q, Chen B, Yankova M, Morest DK, Maryon E, Hand AR, Nonet ML, Wang ZW. Presynaptic ryanodine receptors are required for normal quantal size at the Caenorhabditis elegans neuromuscular junction. J Neurosci. 2005; 25:6745–6754. [PubMed: 16033884]

Liu Q, Hollopeter G, Jorgensen EM. Graded synaptic transmission at the Caenorhabditis elegans neuromuscular junction. Proc Natl Acad Sci U S A. 2009; 106:10823–10828. [PubMed: 19528650]

Maro GS, Gao S, Olechwier AM, Hung WL, Liu M, Ozkan E, Zhen M, Shen K. MADD-4/Punctin and Neurexin Organize C. elegans GABAergic Postsynapses through Neuroligin. Neuron. 2015

Martin JA, Hu Z, Fenz KM, Fernandez J, Dittman JS. Complexin has opposite effects on two modes of synaptic vesicle fusion. Curr Biol. 2011; 21:97–105. [PubMed: 21215634]

Missler M, Hammer RE, Sudhof TC. Neurexophilin binding to alpha-neurexins. A single LNS domain functions as an independently folding ligand-binding unit. J Biol Chem. 1998; 273:34716–34723. [PubMed: 9856994]

Missler M, Zhang W, Rohlmann A, Kattenstroth G, Hammer RE, Gottmann K, Sudhof TC. Alpha-neurexins couple Ca2+ channels to synaptic vesicle exocytosis. Nature. 2003; 423:939–948. [PubMed: 12827191]

Nam CI, Chen L. Postsynaptic assembly induced by neurexin-neuroligin interaction and neurotransmitter. Proc Natl Acad Sci U S A. 2005; 102:6137–6142. [PubMed: 15837930]

Neale BM, Kou Y, Liu L, Ma'ayan A, Samocha KE, Sabo A, Lin CF, Stevens C, Wang LS, Makarov V, et al. Patterns and rates of exonic de novo mutations in autism spectrum disorders. Nature. 2012

Novara F, Beri S, Giorda R, Ortibus E, Nageshappa S, Darra F, Dalla Bernardina B, Zuffardi O, Van Esch H. Refining the phenotype associated with MEF2C haploinsufficiency. Clin Genet. 2010; 78:471–477. [PubMed: 20412115]

Pang ZP, Bacaj T, Yang X, Zhou P, Xu W, Sudhof TC. Doc2 supports spontaneous synaptic transmission by a Ca(2+)-independent mechanism. Neuron. 2011; 70:244–251. [PubMed: 21521611]

Pang ZP, Sun J, Rizo J, Maximov A, Sudhof TC. Genetic analysis of synaptotagmin 2 in spontaneous and Ca2+-triggered neurotransmitter release. Embo J. 2006; 25:2039–2050. [PubMed: 16642042]

Peixoto RT, Kunz PA, Kwon H, Mabb AM, Sabatini BL, Philpot BD, Ehlers MD. Transsynaptic signaling by activity-dependent cleavage of neuroligin-1. Neuron. 2012; 76:396–409. [PubMed: 23083741]

Pettem KL, Yokomaku D, Luo L, Linhoff MW, Prasad T, Connor SA, Siddiqui TJ, Kawabe H, Chen F, Zhang L, et al. The specific alpha-neurexin interactor calsyntenin-3 promotes excitatory and inhibitory synapse development. Neuron. 2013; 80:113–128. [PubMed: 24094106]

Polepalli JS, Wu H, Goswami D, Halpern CH, Sudhof TC, Malenka RC. Modulation of excitation on parvalbumin interneurons by neuroligin-3 regulates the hippocampal network. Nat Neurosci. 2017; 20:219–229. [PubMed: 28067903]

Raghavachari S, Lisman JE. Properties of quantal transmission at CA1 synapses. J Neurophysiol. 2004; 92:2456–2467. [PubMed: 15115789]

Regehr WG, Carey MR, Best AR. Activity-dependent regulation of synapses by retrograde messengers. Neuron. 2009; 63:154–170. [PubMed: 19640475]

Reyes A, Lujan R, Rozov A, Burnashev N, Somogyi P, Sakmann B. Target-cell-specific facilitation and depression in neocortical circuits. Nat Neurosci. 1998; 1:279–285. [PubMed: 10195160]

Richmond JE, Davis WS, Jorgensen EM. UNC-13 is required for synaptic vesicle fusion in C. elegans. Nat Neurosci. 1999; 2:959–964. [PubMed: 10526333]

Rubenstein JL, Merzenich MM. Model of autism: increased ratio of excitation/inhibition in key neural systems. Genes Brain Behav. 2003; 2:255–267. [PubMed: 14606691]

Sabatini BL, Regehr WG. Timing of neurotransmission at fast synapses in the mammalian brain. Nature. 1996; 384:170–172. [PubMed: 8906792]

Saheki Y, Bargmann CI. Presynaptic CaV2 calcium channel traffic requires CALF-1 and the alpha(2)delta subunit UNC-36. Nat Neurosci. 2009; 12:1257–1265. [PubMed: 19718034]

Sara Y, Virmani T, Deak F, Liu X, Kavalali ET. An isolated pool of vesicles recycles at rest and drives spontaneous neurotransmission. Neuron. 2005; 45:563–573. [PubMed: 15721242]

Scheiffele P, Fan J, Choih J, Fetter R, Serafini T. Neuroligin expressed in nonneuronal cells triggers presynaptic development in contacting axons. Cell. 2000; 101:657–669. [PubMed: 10892652]

Simon DJ, Madison JM, Conery AL, Thompson-Peer KL, Soskis M, Ruvkun GB, Kaplan JM, Kim JK. The microRNA miR-1 regulates a MEF-2-dependent retrograde signal at neuromuscular junctions. Cell. 2008; 133:903–915. [PubMed: 18510933]

Suzuki K, Hayashi Y, Nakahara S, Kumazaki H, Prox J, Horiuchi K, Zeng M, Tanimura S, Nishiyama Y, Osawa S, et al. Activity-dependent proteolytic cleavage of neuroligin-1. Neuron. 2012; 76:410–422. [PubMed: 23083742]

Sylwestrak EL, Ghosh A. Elfn1 regulates target-specific release probability at CA1-interneuron synapses. Science. 2012; 338:536–540. [PubMed: 23042292]

Taniguchi H, Gollan L, Scholl FG, Mahadomrongkul V, Dobler E, Limthong N, Peck M, Aoki C, Scheiffele P. Silencing of neuroligin function by postsynaptic neurexins. J Neurosci. 2007; 27:2815–2824. [PubMed: 17360903]

Tong XJ, Hu Z, Liu Y, Anderson D, Kaplan JM. A network of autism linked genes stabilizes two pools of synaptic GABAA receptors. Elife. 2015; 4

Tu H, Pinan-Lucarre B, Ji T, Jospin M, Bessereau JL. C. elegans Punctin Clusters GABA Receptors via Neuroligin Binding and UNC-40/DCC Recruitment. Neuron. 2015

Uemura T, Lee SJ, Yasumura M, Takeuchi T, Yoshida T, Ra M, Taguchi R, Sakimura K, Mishina M. Trans-synaptic interaction of GluRdelta2 and Neurexin through Cbln1 mediates synapse formation in the cerebellum. Cell. 2010; 141:1068–1079. [PubMed: 20537373]

Watanabe S, Liu Q, Davis MW, Hollopeter G, Thomas N, Jorgensen NB, Jorgensen EM. Ultrafast endocytosis at Caenorhabditis elegans neuromuscular junctions. eLife. 2013; 2:e00723. [PubMed: 24015355]

Weber S, Saftig P. Ectodomain shedding and ADAMs in development. Development. 2012; 139:3693–3709. [PubMed: 22991436]

White JG, Southgate E, Thomson JN, Brenner S. The structure of the nervous system of *Caenorhabditis elegans*. Philos Trans R Soc Lond. 1986; 314:1–340. [PubMed: 22462104]

Wittenmayer N, Korber C, Liu H, Kremer T, Varoqueaux F, Chapman ER, Brose N, Kuner T, Dresbach T. Postsynaptic Neuroligin1 regulates presynaptic maturation. Proc Natl Acad Sci U S A. 2009; 106:13564–13569. [PubMed: 19628693]

Highlights

A. Mouse and *C. elegans* α-Neurexins bind CaVα2δ with high affinity

B. *C. elegans* NRX-1 inhibits ACh release by binding to pre-synaptic UNC-36/α2δ

C. SUP-17/ADAM10 cleaves NRX-1 and the shed ectodomain inhibits ACh release

D. Mouse α-Neurexin inhibits the activity of CaV2.2 channels that contain α2δ-3

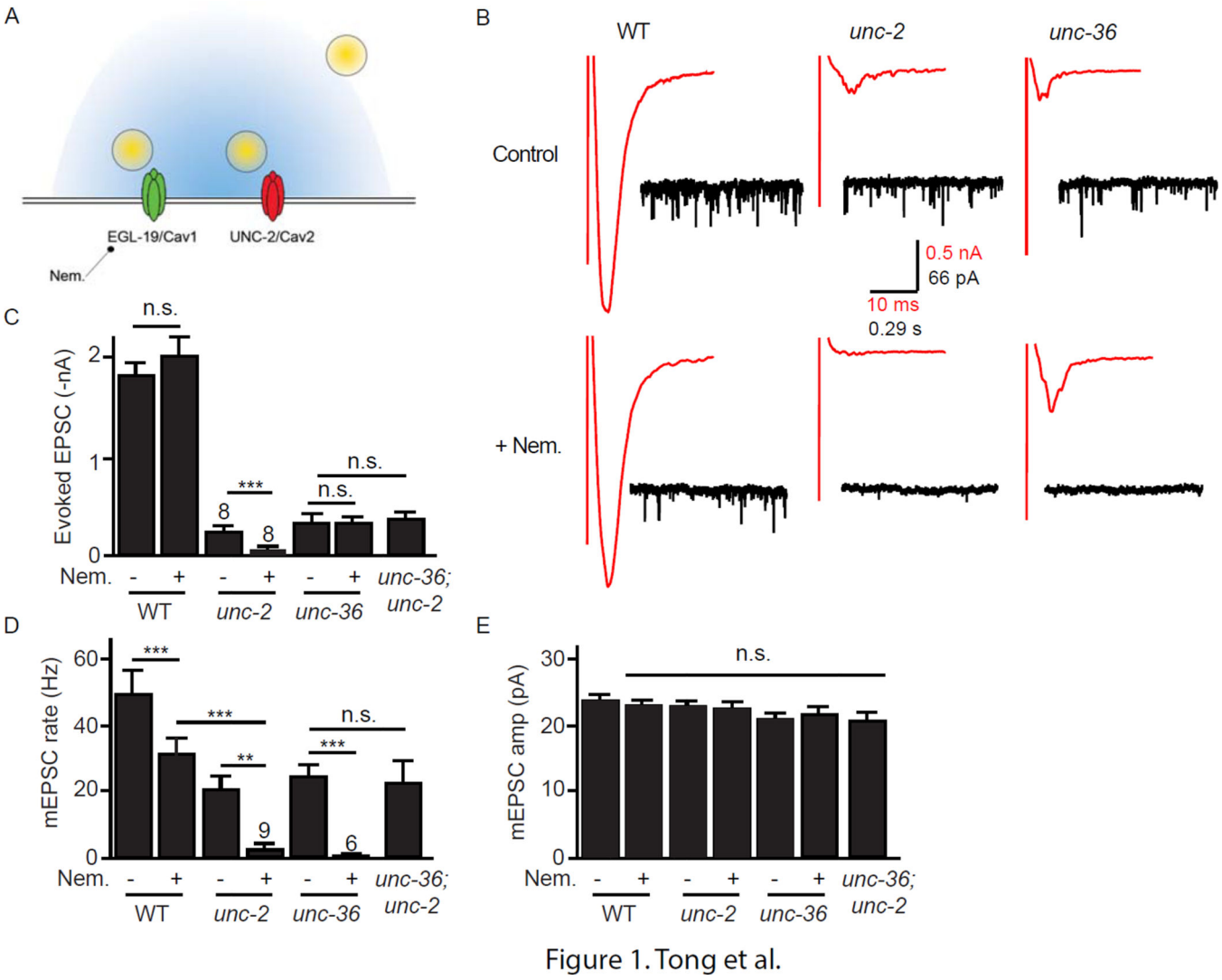

Figure 1. Tong et al.

Figure 1. Effects of UNC-2/CaV2 and EGL-19/CaV1 on evoked and tonic ACh release

(A) A schematic drawing is shown illustrating a cholinergic neuron pre-synaptic nerve terminal. The *C. elegans* genome encodes a single N-type (UNC-2/CaV2) and L-type (EGL-19/CaV1) channel. Release coupled to UNC-2/CaV2 was blocked by recording EPSCs in *unc-2* null mutants. Release coupled to EGL-19/CaV1 was blocked by recording EPSCs in the presence of Nemadipine, an EGL-19 antagonist (Fig. S1). (BE) Evoked ACh release (assessed by recording stimulus-evoked EPSCs) was nearly completely blocked in *unc-2* mutants, whereas Nemadipine treatment had either no effect or modestly reduced evoked responses. By contrast, tonic ACh release (assessed by recording spontaneous mEPSCs) was mediated by both UNC-2/CaV2 and EGL-19/CaV1 channels. Neither *unc-2* mutations nor Nemadapine treatment altered mEPSC amplitudes, suggesting that muscle sensitivity to ACh was unaltered. Averaged evoked responses (red trace) and representative traces of mEPSCs (black trace) in control (above) or nemadipine treated worms (below) are shown for each genotype (B). Mean evoked EPSC amplitude (C), mean mEPSC rate (D), and mean mEPSC amplitudes (E) are shown. Values that differ significantly are indicated

(***, p <0.001; **, p <0.01; n.s., not significant). The number of animals analyzed is indicated for each genotype. Error bars indicate SEM.

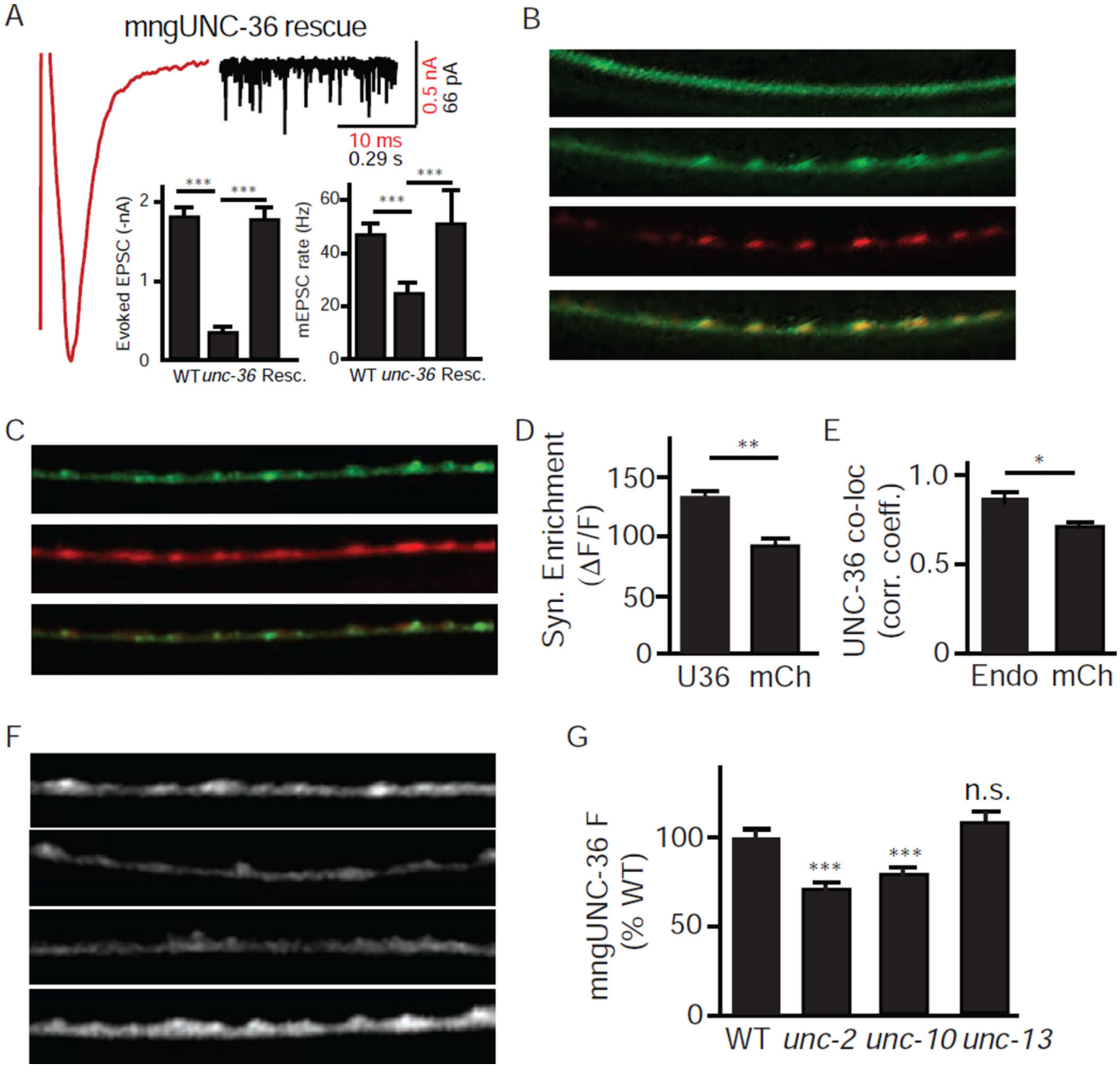

Figure 2. UNC-36/α2δ is an essential auxiliary subunit for UNC-2/CaV2 channels in cholinergic motor neurons

(A) Tonic and evoked ACh release defects of *unc-36* mutants were fully rescued by a transgene expressing mNeonGreen-tagged UNC-36 (mngUNC-36) in all neurons. The averaged evoked EPSC (red trace) and a representative trace of mEPSCs (black trace) in rescued animals, mean evoked EPSC amplitude, and mean mEPSC rate are shown. (B) mngUNC-36 is concentrated at pre-synaptic terminals. When expressed in DA/DB motor neurons, mngUNC-36 exhibited a punctate distribution in dorsal nerve cord (DNC) axons and a diffuse distribution in ventral nerve cord (VNC) dendrites. mngUNC-36 axonal puncta co-localized with a synaptic vesicle marker (mCherry tagged UNC-57/Endophilin). (C–E)

The synaptic enrichment of mngUNC-36 and mCherry (co-expressed in DA/DB neurons) are compared. Representative images (C), ΔF/F of synaptic puncta (D), and Pearson's correlation coefficient of mngUNC-36 with endophilin and mCherry (E) are shown. (F–G) UNC-36 synaptic localization requires endogenously expressed UNC-2/CaV2 channels. mngUNC-36 puncta intensity in DNC axons was significantly decreased in *unc-2* and *unc-10* mutants, but was unaffected in *unc-13* mutants. Representative images (F) and mean puncta intensity (G) are shown for each genotype. Values that differ significantly from wild type controls are indicated (***, $p < 0.001$; **, $p < 0.01$; *, $p < 0.05$; n.s., not significant). The number of animals analyzed is indicated for each genotype. Error bars indicate SEM. Scale bars indicate 10 μm.

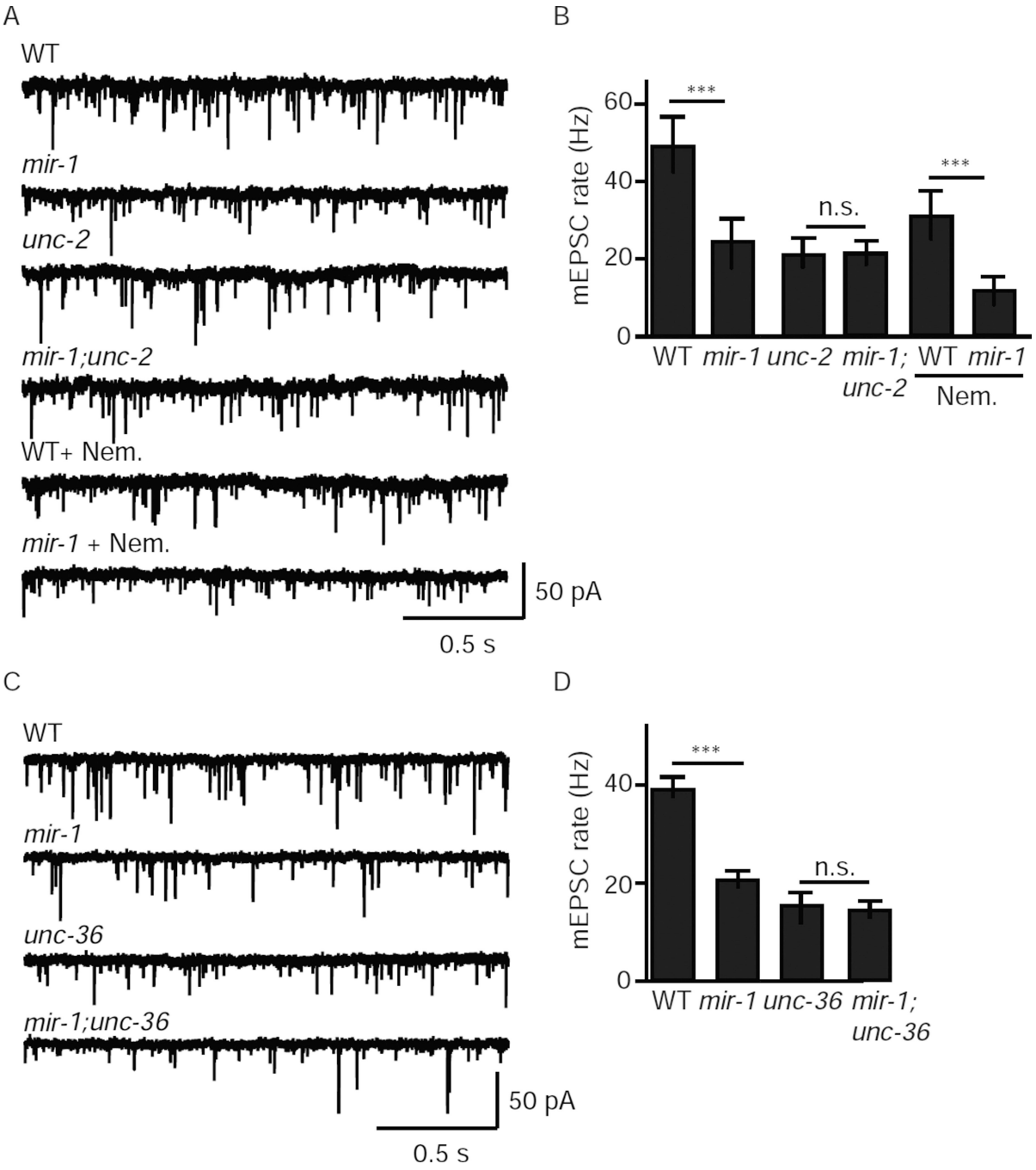

Figure 3. The retrograde signal inhibits tonic release coupled to UNC-2/CaV2 channels

In *mir-1* mutants (where the retrograde signal is activated), tonic release was significant reduced and this effect was blocked by mutations inactivating UNC-2/CaV2 (A–B) and by those inactivating UNC-36/α2δ (C–D) but was unaffected by Nemadipine (an EGL-19/CaV1 antagonist) (A–B). Tonic ACh release was assessed by recording mEPSCs from adult body muscles of the indicated genotypes. Representative mEPSC traces (A,C) and mean mEPSC rates (B,D) are shown. Values that differ significantly are indicated (***, $p < 0.001$;

n.s., not significant). The number of animals analyzed is indicated for each genotype. Error bars indicate SEM.

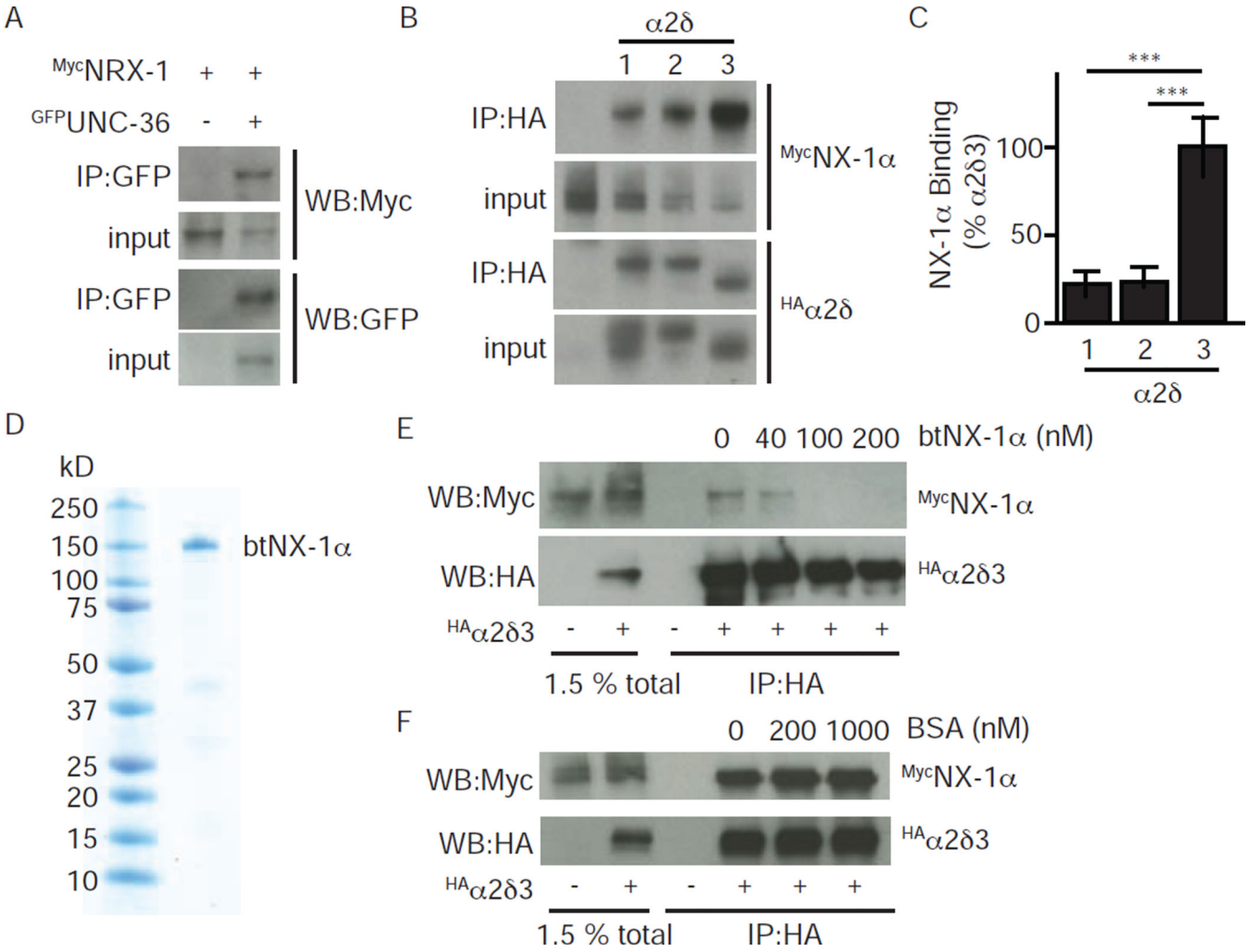

Figure 4. α-NX proteins bind with high affinity to α2δ proteins

α-NX and α2δ proteins carrying the indicated epitope tags were expressed in transfected HEK cells and detected by immunoprecipitation and western blotting. Direct binding interactions were observed between α-NX and α2δ proteins from *C. elegans* (A) and rodents (B–F). Interaction with mouse NX-1α was observed for α2δ-1, 2, and 3 (B–C). Co-immunoprecipitation of rat NX-1α and α2δ-3 was efficiently blocked by adding purified recombinant cow Neurexin (btNX-1α) as a competitor (E). Co-immunoprecipitation was unaffected by adding an unrelated competitor (BSA, F). The ectodomain of btNX-1α was expressed as a soluble secreted protein in insect cells infected with a recombinant baculovirus. A coomassie stained gel of purified btNX-1α is shown (D). Representative gels (A,B,E,F) and quantitation of mouse NX-1α recovery in co-immunoprecipitates (C) are shown. Values that differ significantly are indicated (***, $p < 0.001$; n.s., not significant). Error bars indicate SEM.

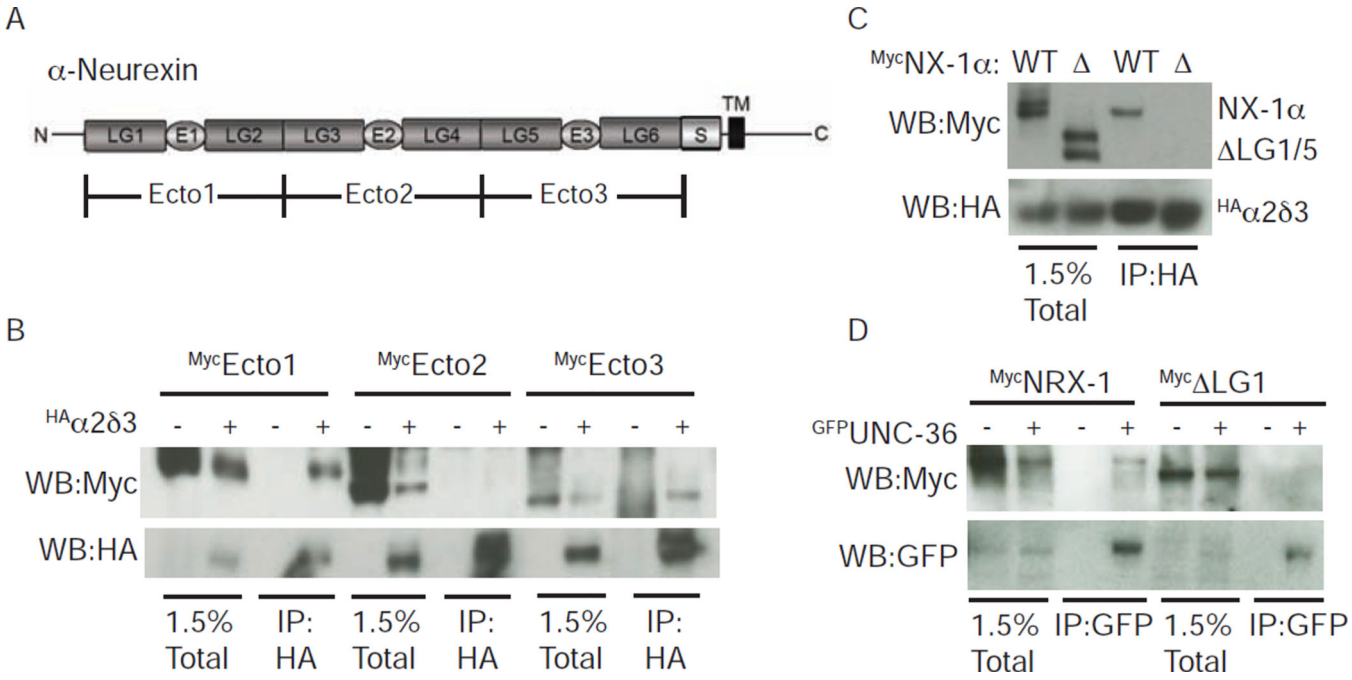

Figure 5. The LG1 and LG5 domains of α-NX mediate binding to α2δ proteins

(A) A schematic is shown illustrating the domains found in α-NX proteins. Laminin-like globular domains (LG1-6), EGF-like domains (E1-3), the stalk region (S), and the transmembrane domain (TM) are indicated. This domain structure is found in mammalian NX-1α and in *C. elegans* NRX-1. Mouse NX-1α ectodomain fragments (Ecto1-3) used to map α2δ binding domains are indicated. (B–D) α-NX domains required for co-immunopreciptation with α2δ binding were mapped using mammalian (B–C) and *C. elegans* (D) proteins. For mouse NX-1α, a mutant lacking these domains (ΔLG1/5) failed to co-immunoprecipitate with α2δ-3 (C). A mutant NRX-1 lacking LG1 (ΔLG1) failed to co-immunoprecipitate with UNC-36/α2δ (D). Proteins carrying the indicated epitope tags were expressed in transfected HEK cells and detected by immunoprecipitation and western blotting. Further mapping of the α-NX binding domains are shown in Fig. S3.

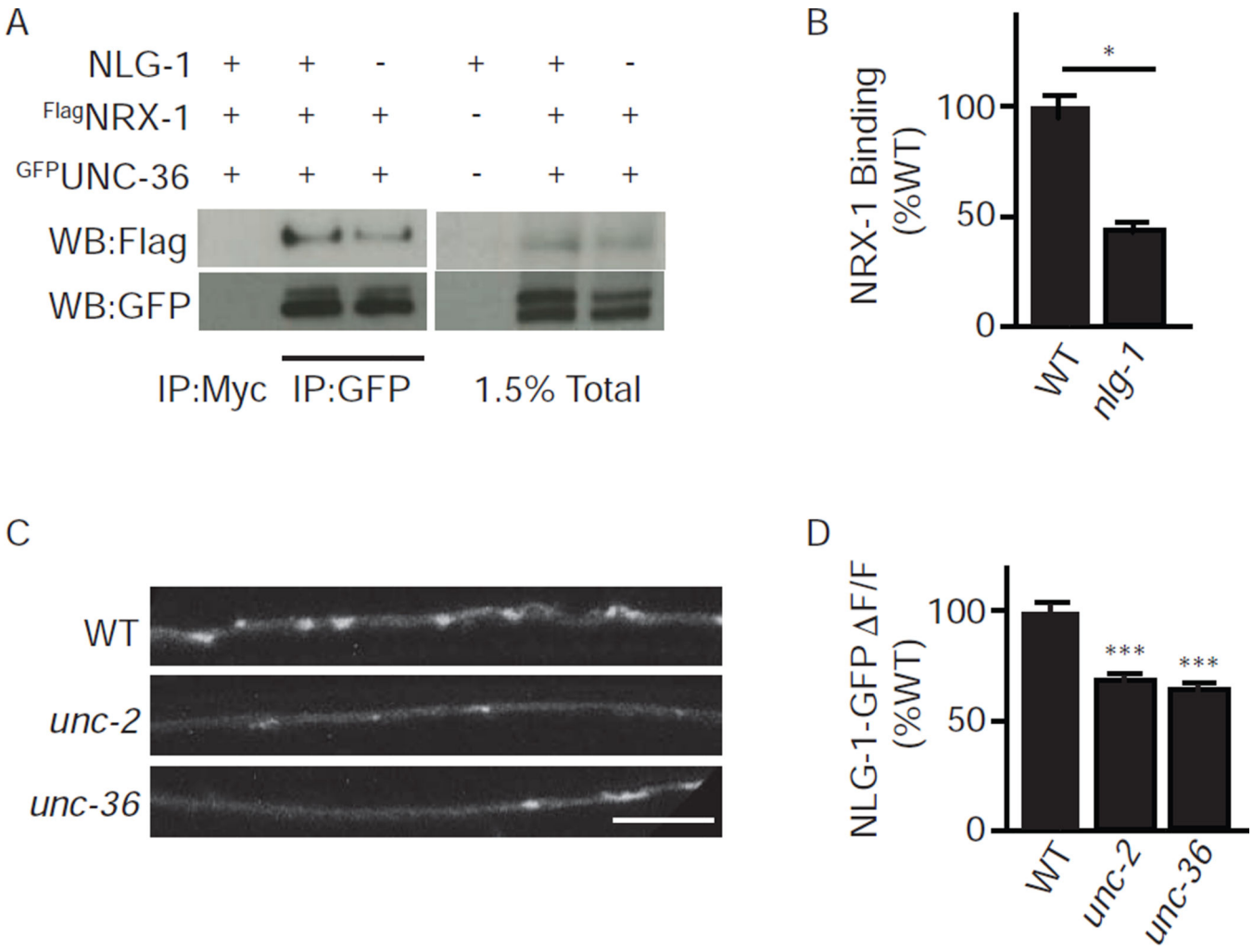

Figure 6. Pre-synaptic NLG-1 promotes NRX-1 binding to UNC-36/α2δ

(A–B) NRX-1 binding to UNC-36 was detected in worm extracts. Membrane extracts were prepared from wild type or *nlg-1* mutant worms that express FLAG-tagged NRX-1 (*myo-3*) and GFP-tagged UNC-36 (*unc-36*), using the indicated promoters. NRX-1 was recovered in immunoprecipitates formed with anti-GFP antibodies but not those formed with an unrelated antibody (anti-MYC). (C–D) NLG-1 synaptic abundance is decreased in mutants lacking UNC-2/CaV2 channels. NLG-1 carrying a cytoplasmic GFP tag (NLG-1-GFP) was expressed in DA/DB motor neurons with the *unc-129* promoter, in animals with the indicated genotypes. Representative images (C) and mean synaptic enrichment (ΔF/F) (D) are shown. Values that differ significantly (***, $p < 0.001$; *, $p < 0.05$). The number of replicate experiments (B) and the number of animals analyzed (D) is indicated for each genotype. Error bars indicate SEM. Scale bar indicates 10 μm.

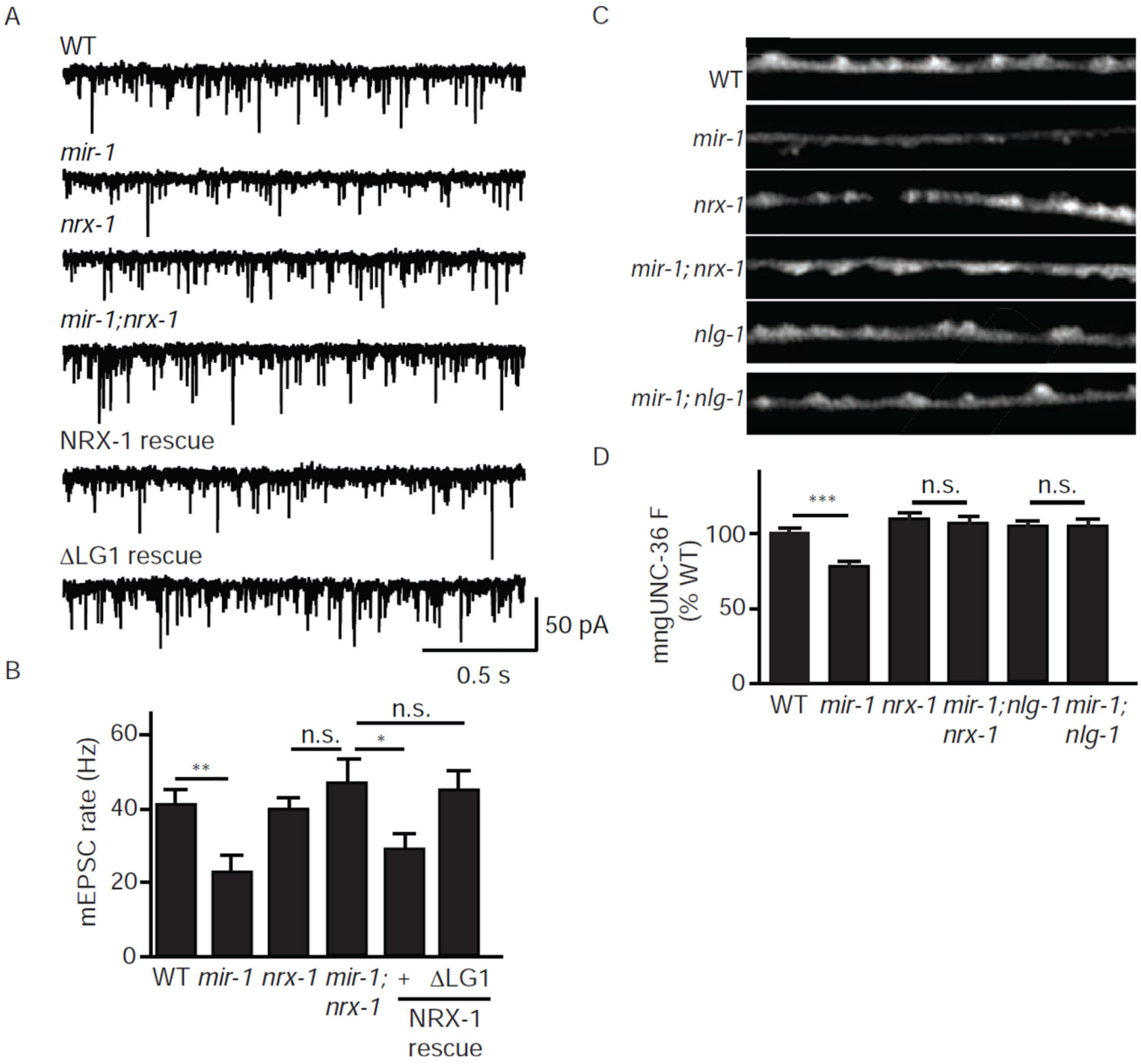

Figure 7. NRX-1 binding to UNC-36/α2δ is required for retrograde inhibition

(A–B) Inhibition of tonic release in *mir-1* mutants (where the retrograde signal is activated) was blocked by mutations inactivating NRX-1. The defect in retrograde inhibition in *mir-1; nrx-1* double mutants was rescued by expressing wild type NRX-1 in body muscles whereas a mutant lacking the LG1 domain (ΔLG1) lacked rescuing activity. Tonic ACh release was assessed by recording mEPSCs from adult body muscles. Representative mEPSC traces (A) and mean mEPSC rates (B) are shown. (C–D) Activating the retrograde signal decreases UNC-36 synaptic abundance. mngUNC-36 puncta intensity in DNC axons was significantly decreased in *mir-1* mutants and this effect was blocked by mutations inactivating NRX-1 and NLG-1 (which block retrograde inhibition). Representative images (C) and mean puncta intensity (D) are shown for each genotype. Values that differ significantly from wild type

controls are indicated (***, $p < 0.001$; **, $p < 0.01$; * $p < 0.05$; n.s., not significant). The number of animals analyzed is indicated for each genotype. Error bars indicate SEM. Scale bar indicates 10 μm.

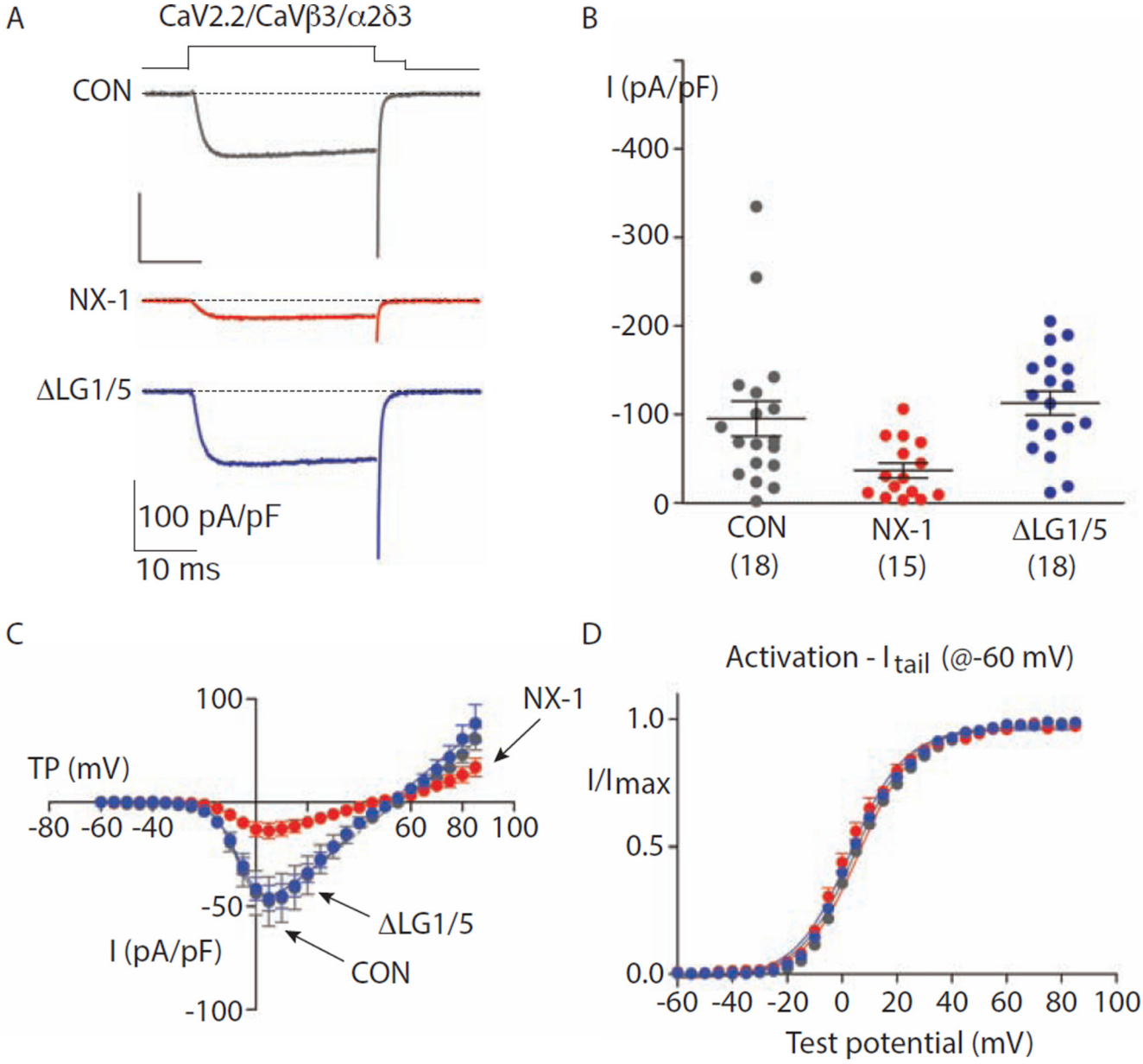

Figure 8. Mouse NX-1α decreases current density of CaV2.2 channels containing α2δ-3

Properties of whole cell CaV2.2 currents recorded from tsA201 cells expressing CaV2.2, CaVβ_3 and α2δ-3 subunits, co-transfected with empty pcDNA3.1 (CON), mouse NX-1α (NX-1α) or mutant NX-1α lacking LG1 and LG5 (ΔLG1/5). All recordings were performed using 1 mM calcium as the charge carrier and the identity of the co-transfected construct was unknown by the experimenter at the time of recording. The experimenter was unblinded after the analysis.

(A) Individual whole cell $Ca_V2.2$ current recordings from three different tsA201 cells expressing CaV2.2, CaVβ_3; and α2δ-3 co-transfected with the indicated constructs. Currents were evoked by 30 ms step depolarization to +10 mV from a holding potential of-100 mV, and tail currents were captured during a 5 ms repolarizing step to −60 mV.

(B) Peak CaV2.2 current densities, evoked by step depolarization to +10 mV from holding potential of -100 mV, from cells co-transfected with the indicated constructs. Each point represents measurement from one cell. Mean and SEM are shown for each condition. The number of cells in each data set is shown in parenthesis below each condition. CON and NX-1α data did not fit a normal distribution, Shapiro-Wilk tests: CON, p = 0.003; NX-1α, p = 0.05; and ΔLG1/5, p = 0.83. Non-parametric Kruskal-Wallis test (KW) with Dunn's multiple pairwise testing (DMP) were as follows: CON vs NX-1α, p = 0.0006 (KW) and p = 0.0399 (DMP); CON vs ΔLG1/5, p = 0.4833 (KW); and ΔLG1/5 vs NX-1α, p = 0.0004 (KW). Indicating that NX-1α co-expression significantly reduced peak current densities.
(C) Average peak CaV2.2 current voltage (I–V) relationships measured in cells co-transfected with CON (n = 17), NX-1α (n = 13), and ΔLG1/5 (n = 12). Currents were evoked by depolarizing steps of increasing amplitudes in 5 mV intervals from a holding potential of −100 mV. Boltzmann-linear functions were fit to individual data sets from each cell and used to estimate activation mid-point ($V_{1/2}$), slope factor (k) and reversal potential (V_{rev}) in Table S1.
(D) Activation curves generated from peak tail CaV2.2 current amplitudes captured at −60 mV plotted against the value of the preceding test depolarization in cells co-transfected with CON (n = 14), NX-1α (n = 9), and ΔLG1/5 (n = 10). Voltage steps were applied every 10 sec, in 5 mV increments, between −60 and +85 mV. I/Imax was measured for tail currents over the range of test potentials. Boltzmann functions were fit to data from each cell and average $V_{1/2}$ and k values estimated and documented in Table S1. CaV2.2 activation curves were not distinguishable across these conditions.

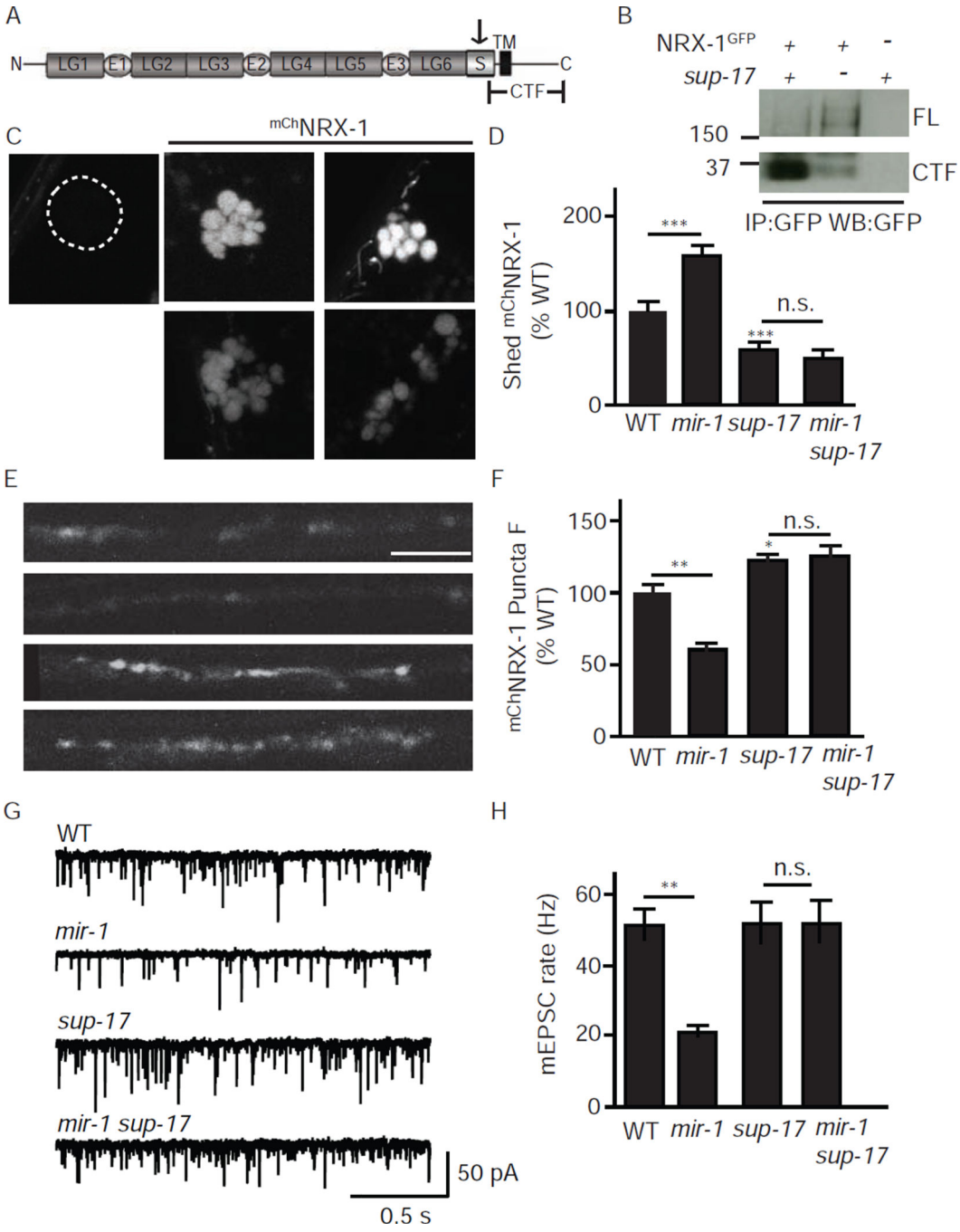

Figure 9. Retrograde inhibition is mediated by a soluble form of the NRX-1 ectodomain

(A) A schematic drawing is shown illustrating the domains found in α-NX proteins. The arrow indicates the location of the predicted SUP-17/ADAM10 cleavage site in the stalk domain. The carboxy-terminal fragment (CTF) produced by proteolytic cleavage is indicated. (B) SUP-17/ADAM10 cleaves NRX-1 in the stalk region. NRX-1 containing a cytoplasmic GFP tag (NRX-1^{GFP}) was expressed in body muscles. NRX-1^{GFP} cleavage was assayed by analyzing the abundance of full length (FL) and the CTF fragment of NRX-1 in western blots of membrane extracts. In *sup-17* mutants, FL-NRX-1 abundance was increased

and CTF abundance was decreased, both indicating decreased NPvX-1 cleavage. (C–F) NRX-1 ectodomain shedding is increased when the retrograde signal is activated. NRX-1 containing an mCherry tag in the ectodomain (^{mCh}NRX-1) was expressed in body muscles. Shedding of ^{mCh}NRX-1's ectodomain was assayed by analyzing mCherry fluoresence in the endolysosomal compartment of coelomocytes (C–D). Coelomocyte fluorescence was not detected in animals expressing the cytoplasmically tagged NRX-1^{GFP} (C). Intact (uncleaved) ^{mCh}NRX-1 molecules were assayed by analyzing the fluorescent intensity of mCherry puncta in the dorsal nerve cord (E–F). When the retrograde signal was activated (in *mir-1* mutants), coelomocyte fluorescence was significantly increased (C–D) while dorsal cord fluorescence was decreased (E–F), both indicating increased NRX-1 shedding. The increased NRX-1 shedding observed in *mir-1* mutants was abolished in *mir-1 sup-17* double mutants. Representative images (C,E), mean coelomocyte fluorescence (D), and mean dorsal cord puncta intensity (F) are shown. (G–H) Retrograde signaling is blocked in *sup-17* ADAM10 mutants. Tonic ACh release was assessed by recording mEPSCs from adult body muscles. Representative traces (G) and mean mEPSC rates (H) are shown. Activating the retrograde signal (in *mir-1* mutants) decreases the mEPSC rate and this effect was blocked in *mir-1 sup-17* double mutants. For all experiments involving the *sup-17(n1258ts)* mutation, mutant and contemporaneous controls were grown at the non-permissive temperature (25°C). Values that differ significantly are indicated (***, $p < 0.001$; **, $p < 0.01$; as., not significant). The number of animals analyzed is indicated for each genotype. Error bars indicate SEM. Scale bar indicates 10 μm.